J. Fluid Mech. (1992), *vol.* 238, *pp.* 405–433
Printed in Great Britain

Assessment of two-equation models of turbulent passive-scalar diffusion in channel flow

By KIYOSI HORIUTI

Institute of Industrial Science, University of Tokyo, 7-22-1 Roppongi, Minato-ku, Tokyo 106, Japan

(Received 2 October 1990 and in revised form 3 September 1991)

Models for the transport of passive scalar in turbulent flow were investigated using databases derived from numerical solutions of the Navier–Stokes equations for fully developed plane channel flow, these databases being generated using large-eddy and direct numerical simulation techniques. Their reliability has been established by comparison with the experimental measurements of Hishida, Nagano & Tagawa (1986). The present paper compares these simulations and calculations using the Nagano & Kim (1988) 'two-equation' model for the scalar variance (k_θ) and scalar variance dissipation (ϵ_θ). This model accounts for the dependence of flow quantities on the Prandtl number by expressing eddy diffusivity in terms of the ratio of the timescales of velocity and scalar fluctuations. However, the statistical analysis by Yoshizawa (1988) showed that there was an inconsistency in the definition of the isotropic eddy diffusivity in the Nagano–Kim model, the implications of which are clearly demonstrated by the results of this paper where large-eddy simulation and direct numerical simulation (LES/DNS) databases are used to compute the quantities contained in both models. An extension of the Nagano–Kim model is proposed which resolves these inconsistencies, and a further development of this model is given in which the anisotropic scalar fluxes are calculated. Near a rigid surface, a third-order 'anisotropic representation' of scalar fluxes may be used as an alternative model for reducing the eddy diffusivity, instead of the conventional 'damping functions'. This model is similar but distinct from the algebraic scalar flux model of Rogers, Mansour & Reynolds (1989). A third aspect of this paper is the use of the LES/DNS databases to evaluate certain coefficients (those for modelling the pressure–scalar gradient terms) of another model of a similar type, namely the algebraic scalar flux model of Launder (1975).

1. Introduction

Turbulent diffusion of passive scalar is an important, complex field in science and engineering, and following increases in computation abilities of computers, it has become possible to analyse this type of diffusion by numerically integrating the governing equations. The most commonly adopted methods involve the use of the k–ϵ model which expresses the eddy diffusivity of the scalar field by prescribing the turbulent Prandtl number (Pr_t), where in this model k denotes the turbulent kinetic energy and ϵ is the dissipation rate of k. However, these methods subsequently need an empirical formula for Pr_t, lack application universality, and do not include a molecular Prandtl-number (Pr) dependence.

Another approach reported by Nagano & Kim (1988, hereinafter referred to as NK) employed scalar variance (k_θ) and scalar variance dissipation (ϵ_θ) equations, and

prescribed the eddy diffusivity using these quantities, thereby avoiding phenomenological assumptions for Pr_t. This proposed model was tested in both a flat-plate boundary layer and at a thermal entrance region of a pipe, yielding satisfactory results for a wide range of Pr (0.1–10000). In defining eddy diffusivity, a timescale of scalar fluctuation must be specified, with this scale usually being determined by combining the dynamic timescale expressed by k and ϵ and the scalar timescale expressed by k_θ and ϵ_θ. The resulting eddy diffusivity can then be rewritten as the product of the conventional eddy viscosity of the velocity field and the ratio (r) of these two timescales taken to the exponent p. NK determined that the exponent should be $-\frac{1}{2}$, whereas Yoshizawa (1988) statistically found that it should be equal to -2. The difference in the exponent value led to the present study which focuses on resolving this inconsistency.

Several techniques for turbulent-flow numerical simulations are presently in use, i.e. Reynolds-averaged numerical simulations (RANS), large-eddy simulations (LES), and direct numerical simulations (DNS). In RANS, averaging is done in both space and time over several turnover timescales of large eddies, whereas in LES it is done in scales encompassing grid intervals (subgrid scales (SGS)). DNS on the other hand, resolves all the scales up to or close to the Kolmogorov dissipation scale and uses no turbulence models, although its applications have been limited to simple geometries, e.g. plane channel flow, at relatively low Reynolds numbers (Kim, Moin & Moser 1987). However, further assumptions are required in LES and RANS to relate the correlations in the unresolved scale to the resolved scale variables, with their assessment having been performed using more elementary levels of numerical simulation data. Clark, Ferziger & Reynolds (1977), Bardina, Ferziger & Reynolds (1980), Piomelli, Moin & Ferziger (1988), and Horiuti (1989) employed LES turbulence models which were directly tested by a comparison with DNS data. Improved models, having a higher correlation with DNS data, have been studied in *a posteriori* tests which incorporate these models into actual LES computations, where significant improvements were obtained in turbulence statistics. In addition, a DNS database has been used to evaluate RANS models (Mansour, Kim & Moin 1988). Since channel flow DNS analysis has only been done at low Reynolds numbers, only a small fraction of the logarithmic layer is discernible in the mean velocity profile (Kim *et al.* 1987), with results indicating that it is a suitable technique to evaluate the models for simulating the near-wall region. LES is applicable at higher Reynolds numbers where extensive tests of RANS models in the logarithmic layers are possible using the LES database. The DNS database is, however, more reliable in evaluating the higher-order statistics required for the evaluation of turbulence models.

The major objective here is to assess the two-equation model and determine the exponent p using the LES and DNS databases for plane channel flow. To generate the LES database, models are incorporated which approximate the cross-terms between the grid scale (GS) and SGS velocity components terms arising during filtering of the Navier–Stokes equations. The Bardina model, based on a scale similarity hypothesis (Bardina *et al.* 1980), was adopted for the models of cross-terms because previous direct tests of LES models in plane channel flow (Piomelli *et al.* 1988; Horiuti 1989) revealed that the Bardina model provides an accurate approximation for the cross-terms, and also because neglecting them degrades the computation. The cross-terms in the filtered scalar transport equations, i.e. the correlation between the GS velocity and SGS scalar components and vice versa, have been approximated here in the same manner, with subsequent database reliability

being tested by comparing results with experimental measurements of Hishida, Nagano & Tagawa (1986). By including these models for the cross-terms, overall statistics were significantly improved, e.g. the mean scalar profile. It is not yet clear whether the LES database statistics are reliable for the evaluation of turbulence models, thus three simulations were accordingly conducted: two LES cases using different grid resolutions and one DNS case. Additionally, two methods were tested which drive the passive scalar field. When these LES/DNS databases were used to compute the quantities contained in the two-equation models, it was revealed that two-equation models based on either $p = -2$ or $-\frac{1}{2}$ are quite inaccurate in the region where r varies considerably, and that a $p = 1 \sim 3$ model yields better results.

As an inevitable consequence of using isotropic eddy viscosity/diffusivity representations, conventional two-equation models fail to predict the anisotropy of Reynolds stresses and scalar fluxes. Leslie (1973) devised a representation of anisotropy of scalar fluxes to circumvent this drawback, and Yoshizawa (1988) extended Leslie's work by showing that this representation yields a good approximation for the anisotropy of scalar fluxes in comparison with the experimental measurements of Tavoularis & Corrsin (1981). Recently, Rubinstein & Barton (1991) applied renormalization group theory to compute anisotropic corrections to eddy diffusivity, and then derived similar anisotropic models. Similarly to isotropic eddy diffusivity, anisotropic representation of scalar flux also involves the exponent p, with corresponding evaluation of p being done via these fluxes. The second-order models adopted by Newman, Launder & Lumley (1981) and Elgobashi & Launder (1983) provide an alternative approach to model an anisotropy of scalar fluxes by avoiding the empirical assumption on Pr_t. These models directly solve the transport equations of scalar fluxes, being further simplified by Gibson & Launder (1976) to yield algebraic relations among these fluxes. The resulting algebraic scalar flux models (AFM) were tested by Rogers, Mansour & Reynolds (1989 hereinafter referred to as RMR) using the DNS databases for homogeneous shear and plane channel flows. Horiuti (1990) reported that third-order representation of anisotropy may be used as an alternative method for calculating the Reynolds stresses near the wall. This can replace the conventional Van Driest damping function (Van Driest 1956) which is commonly used in k–ϵ models. The present paper discusses the use of third-order representation of anisotropy for scalar fluxes to reduce the eddy diffusivity near a rigid surface. Its similarities and differences with AFM (RMR 1989) is further discussed. It is known that all turbulent models must be tested by incorporating them into actual computations, however, the present paper primarily deals with the tests of models by comparing their correlations with numerical databases.

The governing equations and selected LES turbulence models are briefly described in §2, whereas §3 presents the two-equation model for passive-scalar diffusion by NK, and shows several database profiles which demonstrate the reliability of LES/DNS databases. The two-equation model is subsequently assessed in §4 using the generated databases, and a new model that mitigates the drawbacks in the previous models is proposed. A critical comparison with AFM is then made in §5, with §6 containing a summary and conclusions.

2. The governing equations/LES models

Incompressible channel flow is considered using the Navier–Stokes, continuity and passive-scalar transport governing equations, with the LES basic equations for the

filtered velocity components $\bar{u}_i (i = 1,2,3)$, the filtered pressure $\bar{p}$, and the filtered scalar $\bar{\theta}$, being

$$\frac{\partial \bar{u}_i}{\partial t} + \frac{\partial}{\partial x_j}(\bar{u}_i \bar{u}_j) = -\frac{\partial}{\partial x_j}\tau_{ij} - \frac{\partial \bar{p}}{\partial x_i} + \frac{1}{Re}\Delta \bar{u}_i + 2\delta_{i1}, \tag{1}$$

$$\frac{\partial \bar{u}_i}{\partial x_i} = 0, \tag{2}$$

$$\frac{\partial \bar{\theta}}{\partial t} + \frac{\partial}{\partial x_j}(\bar{u}_j \bar{\theta}) = -\frac{\partial}{\partial x_j}\tau_j^{\theta} + \kappa \Delta \bar{\theta} + Q^0, \tag{3}$$

where δ_{ij} is the Kronecker delta symbol, Q^0 the volumetric scalar source term, and κ the scalar diffusivity. Equations (1)–(3) and their variables are filtered by applying a two-dimensional Gaussian filter in the $i = 1,3$ directions, and a top-hat filter in the $i = 2$ direction (Moin & Kim 1982; Horiuti 1987), where $i = 1,2,3$, respectively correspond to directions x, y and z, with x being the downstream coordinate, y the normal coordinate, and z the spanwise coordinate. Unfiltered variables are denoted by u_i, p, θ and SGS components by $u_i^{\mathrm{SGS}}, p^{\mathrm{SGS}}, \theta^{\mathrm{SGS}}$, i.e. $u_i = \bar{u}_i + u_i^{\mathrm{SGS}}$, $p = \bar{p} + p^{\mathrm{SGS}}$, $\theta = \bar{\theta} + \theta^{\mathrm{SGS}}$, and occasionally, $u_i (i = 1,2,3)$ is respectively denoted by u, v, w. In the DNS governing equations, filtered variables in (1)–(3) are replaced by the raw variables u_i, p, θ, and τ_{ij} and τ_j^{θ} are eliminated. The flow is driven by the mean pressure gradient, and all variables have been made dimensionless using the channel width (H), the friction velocity (u_τ), and the friction scalar (θ_τ), unless otherwise stated. The Reynolds number Re is defined by $u_\tau H/\nu$ (ν is the kinematic viscosity), the length given in wall units is denoted by $(\,)_+$, and the Prandtl number Pr is set equal to 0.7. In (1) and (3), τ_{ij} and τ_j^{θ} are

$$\tau_{ij} = (\overline{\bar{u}_i \bar{u}_j} - \bar{u}_i \bar{u}_j) + (\overline{\bar{u}_i u_j^{\mathrm{SGS}} + u_i^{\mathrm{SGS}} \bar{u}_j}) + \overline{u_i^{\mathrm{SGS}} u_j^{\mathrm{SGS}}}, \tag{4a}$$

$$\tau_j^{\theta} = (\overline{\bar{u}_j \bar{\theta}} - \bar{u}_j \bar{\theta}) + (\overline{\bar{u}_j \theta^{\mathrm{SGS}} + u_j^{\mathrm{SGS}} \bar{\theta}}) + \overline{u_j^{\mathrm{SGS}} \theta^{\mathrm{SGS}}}. \tag{4b}$$

The first terms in the right-hand side of (4a) and (4b) are the Leonard terms explicitly calculated by applying the Gaussian filter in the x and z directions in the Fourier space. The next terms are the cross-terms, and the last ones the SGS Reynolds stresses and SGS scalar fluxes. The Bardina model (Bardina *et al.* 1980) approximates the second and last terms in τ_{ij} as

$$(\overline{\bar{u}_i u_j^{\mathrm{SGS}} + u_i^{\mathrm{SGS}} \bar{u}_j}) + \overline{u_i^{\mathrm{SGS}} u_j^{\mathrm{SGS}}} \sim \bar{u}_i \bar{u}_j - \bar{\bar{u}}_i \bar{\bar{u}}_j. \tag{5}$$

This model is based on a scale similarity hypothesis, having been adopted to approximate the second and last terms in τ_j^{θ} as

$$(\overline{\bar{u}_j \theta^{\mathrm{SGS}} + u_j^{\mathrm{SGS}} \bar{\theta}}) + \overline{u_j^{\mathrm{SGS}} \theta^{\mathrm{SGS}}} \sim \bar{u}_j \bar{\theta} - \bar{\bar{u}}_j \bar{\bar{\theta}}. \tag{6}$$

Since the Bardina model does not dissipate sufficient turbulent energy (Bardina *et al.* 1980; Piomelli *et al.* 1988; Horiuti 1989), the Smagorinsky model (Smagorinsky 1963) was used for the SGS Reynolds stresses,

$$\overline{u_i^{\mathrm{SGS}} u_j^{\mathrm{SGS}}} = \tfrac{1}{3}\overline{u_l^{\mathrm{SGS}} u_l^{\mathrm{SGS}}}\,\delta_{ij} - \nu_e^{\mathrm{LES}} e_{ij}, \tag{7}$$

$$\nu_e^{\mathrm{LES}} = (C_{\mathrm{S}}\Delta)^2 [\tfrac{1}{2} e_{ij} e_{ij}]^{\frac{1}{2}}, \quad e_{ij} = \frac{\partial \bar{u}_i}{\partial x_j} + \frac{\partial \bar{u}_j}{\partial x_i},$$

being added to (5) with the Smagorinsky constant $C_{\mathrm{S}} = 0.1$. The SGS scalar flux in (4b) is approximated by,

$$\overline{u_i^{\mathrm{SGS}} \theta^{\mathrm{SGS}}} = -\kappa_e^{\mathrm{LES}} \frac{\partial \bar{\theta}}{\partial x_i}, \quad \kappa_e^{\mathrm{LES}} = (C_{\mathrm{S}\theta}\Delta)^2 [\tfrac{1}{2} e_{ij} e_{ij}]^{\frac{1}{2}}, \tag{8}$$

with $C_{S\theta} = 0.14$. The same SGS model was used by Antonopoulos-Domis (1981) for LES of passive scalar diffusion in isotropic turbulence, where $C_S/C_{S\theta}$ were chosen equal to 0.23/0.32. It should be noted that a larger C_S value has been used for isotropic turbulence than for channel flow (e.g. Clark *et al.* 1977; Horiuti 1991*a*). In both the present study and Antonopoulos-Domis (1981), the $C_{S\theta}/C_S$ ratio is ≈ 1.4, giving an approximate SGS turbulent Prandtl number of 0.6. The lengthscale Δ in (7)–(8) is defined as $(\Delta x \Delta y \Delta z)^{\frac{1}{3}}$, with $\Delta x, \Delta y, \Delta z$ being the mesh sizes in the x, y, z directions, followed by multiplying these terms by the Van Driest damping function (Van Driest 1956; $1-\exp(-y_+/A_+)$, $A_+ = 26$), which ensures that (7)–(8) are compatible with the boundary conditions for velocity and scalar fluctuations at the walls. In the RANS models, a slightly larger value of A_+ is normally adopted for the damping function of eddy diffusivity at $Pr = 0.7$ (NK 1988), with computed results in the present LES data being rather insensitive to small perturbations of A_+. For the sake of simplicity, the same A_+ value was adopted here, although the two-part model in Schumann (1975), Grötzbach & Schumann (1979), and Moin & Kim (1982) was not utilized. (This two-part model is further discussed in §3.) The validation of SGS models for passive-scalar diffusion LES was previously shown in Horiuti (1991*b*).

Periodic boundary conditions are imposed in the homogeneous directions (x and z) for velocity, pressure and scalar, with a no-slip boundary condition for velocity being imposed at the walls. Two types of wall boundary conditions were chosen for the scalar, i.e. in Type I,

$$\bar{\theta} = 0 \quad \text{at the walls,} \tag{9a}$$

$$Q^0 = 2 \quad \text{inside the channel region,} \tag{9b}$$

with the scalar uniformly input within the fluid and then removed at both walls. In Type II,

$$\bar{\theta} = 1 \quad \text{at the lower wall,} \tag{10a}$$

$$\bar{\theta} = 0 \quad \text{at the upper wall,} \tag{10b}$$

$$Q^0 = 0. \tag{10c}$$

In this case, the scalar was input to the flow at one wall and removed at the other, with all Type II results being renormalized using θ_τ (§4). This is too complex an experiment to be done for plane-channel-flow conditions of Type I, however, Type I is very similar to the heat-transfer models in the pipe flow when its circumference is uniformly heated (Hishida *et al.* 1986). The Type II boundary conditions were the same conditions used to combine free and forced convection between vertical parallel plates (Nakajima *et al.* 1980), and also used in the same flow configuration that Tsai, Voke & Leslie (1987) used for large eddy simulation.

To numerically solve (1)–(3), a pseudospectral method using Fourier series expansion was used to approximate the spatial derivatives in the x- and z-directions, whereas for the y-direction a second-order central finite-difference method was used in LES, and for DNS, the Chebyshev polynomial expansion method. Aliasing errors were removed by using the $\frac{3}{2}$-rule, and time integration was done by combining the Adams–Bashforth and Crank–Nicolson methods (Horiuti 1987). Table 1 summarizes the experimental cases considered. The grid intervals in wall units in the x/z directions for Cases 1 and 2 were 32/16, Cases 3 and 4 were 64/32, and Case 5 was 18/9 (see Kim 1988). The initial grid point in the y-direction was located at 0.83 for Cases 1 and 2, 1.8 for Cases 3 and 4, and 0.054 for Case 5. The time interval Δt was 0.0001 for LES and 0.00025 for DNS, being chosen so as to strictly adhere to the Courant number

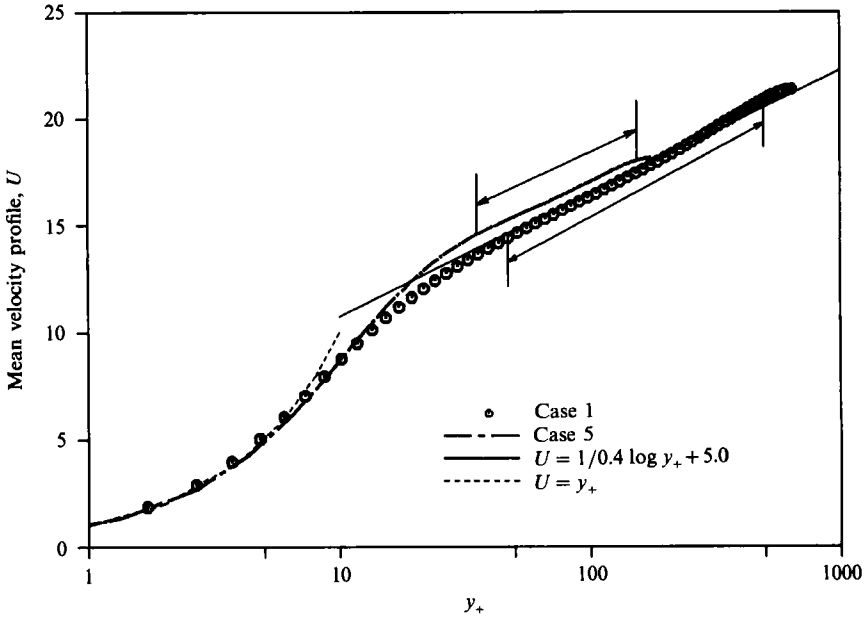

FIGURE 1. Mean streamwise velocity profile. Only the data in the region shown between the arrows was used for the least-squares fitting in §4.

Case	Grid parameters	Numerical method	Re	Scalar field boundary condition	Computational domain size	
					Streamwise	Spanwise
1	$128 \times 129 \times 128$	LES	1280	I	$3.2H$	$1.6H$
2	$128 \times 129 \times 128$	LES	1280	II	$3.2H$	$1.6H$
3	$64 \times 62 \times 64$	LES	1280	I	$3.2H$	$1.6H$
4	$64 \times 62 \times 64$	LES	1280	II	$3.2H$	$1.6H$
5	$128 \times 129 \times 128$	DNS	360	I	$6.4H$	$3.2H$

TABLE 1. Case specifications

limitation. After a fully developed state was reached, integration times for ensemble averaging of statistical value were 2.5 for Cases 1, 3–5 and 1.0 for Case 2. A portion of the Case 1 and 2 turbulence statistics was reported in Horiuti (1988, 1990).

Figure 1 shows the mean streamwise velocity profiles, and a fairly long region fitting the logarithmic law appears in Case 1. Both the von Kármán constant (0.4) and a constant B (5.0) (Hinze 1959) in Case 1 correlate well with the experiments of Hussain & Reynolds (1975). $B(\sim 5.5)$ in Case 5 is in good agreement with Kim *et al.* (1987). To ensure this computation was in equilibrium, the average Reynolds shear stress profile from Case 1 is shown in figure 2, i.e. a summation of the GS mean Reynolds stress $\langle \bar{u}'' \bar{v} \rangle$ and the contribution of the Bardina model $\langle \bar{u}\bar{v} - \bar{\bar{u}}\bar{\bar{v}} \rangle$. The (x, z)-plane and the time average are shown, and $\bar{u}_i''$ is a deviation of $\bar{u}_i$ from the (x, z)-plane average. Figure 2 additionally shows the total stress in which the SGS terms and molecular stress are included. The total stress is balanced by the mean pressure gradient, thus indicating the computation is in statistical equilibrium. The contribution of the SGS Reynolds stress terms from Cases 1 and 3 are included in figure 2, where it should be noticed that the sign and magnitude of these terms has changed,

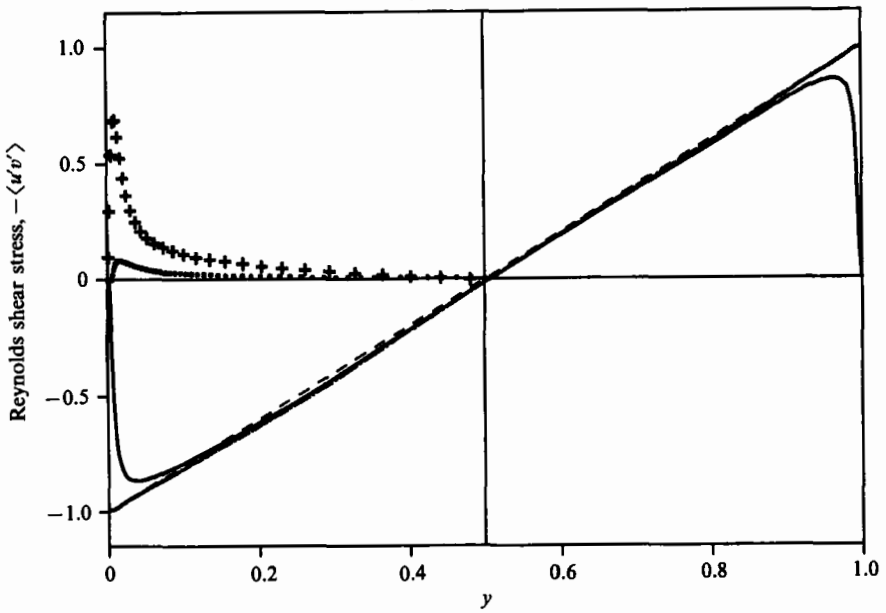

FIGURE 2. Mean Reynolds shear stress: ——, GS stress $\langle \bar{u}'' \bar{v} \rangle + \langle \overline{uv} - \bar{u}\bar{v} \rangle$ from Case 1; — · —, total shear stress from Case 1; ●, SGS terms from Case 1 (factored by 5.0) $\langle \nu_e^{\text{LES}} [(\partial \bar{u}/\partial y) + (\partial \bar{v}/\partial x)] \rangle$; +, SGS terms from Case 3 (factored by 5.0) $\langle \nu_e^{\text{LES}} [(\partial \bar{u}/\partial y) + (\partial \bar{v}/\partial x)] \rangle$.

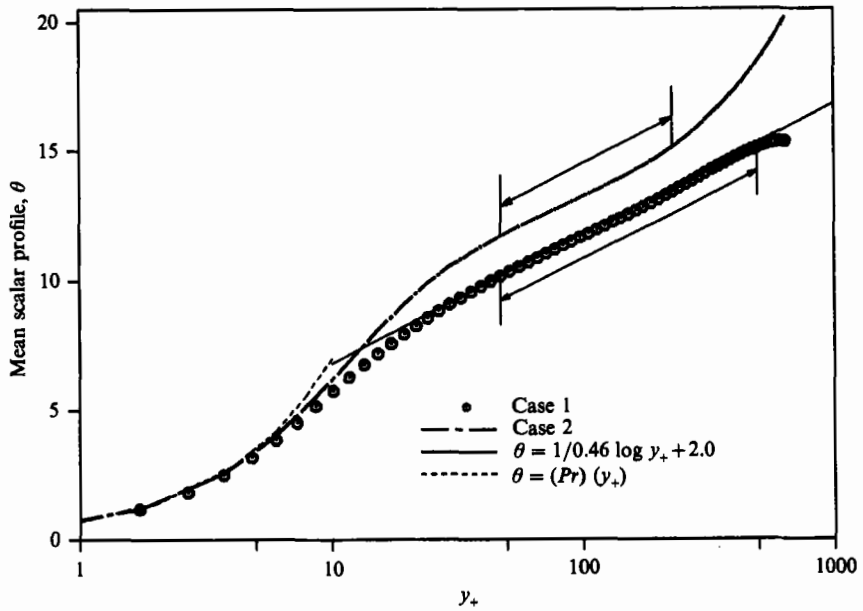

FIGURE 3. Mean scalar profile. Only the data in the region shown between the arrows were used for the least-squares fitting in §4.

indicating for Case 1 that most momentum and scalar transport contributions have been carried out by the GS part, with the SGS terms' contribution being less than 2% of the total Reynolds shear stress. On the other hand, their contribution in Case 3 is very significant in the vicinity of the wall. Figure 3 shows the mean scalar profile from Cases 1 and 2, and the logarithmic profile is clearly evident. Figures 1 and 3 give

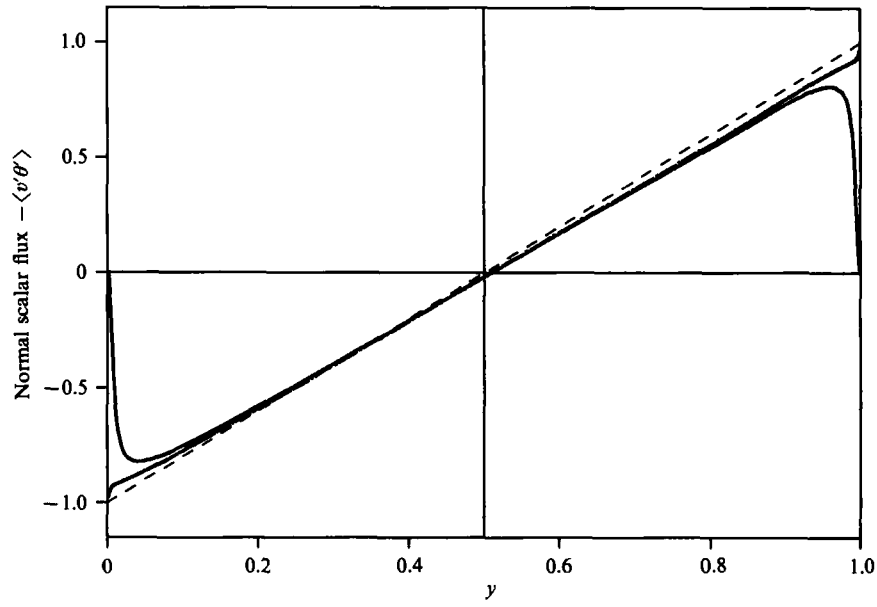

FIGURE 4. Mean normal scalar flux from Case 1. —, GS flux $\langle \bar{u}_2''\bar{\theta}''\rangle + \langle \bar{u}_2\bar{\theta} - \bar{\bar{u}}_2\bar{\bar{\theta}}\rangle$; —·—, total scalar flux; ---, scalar source flux.

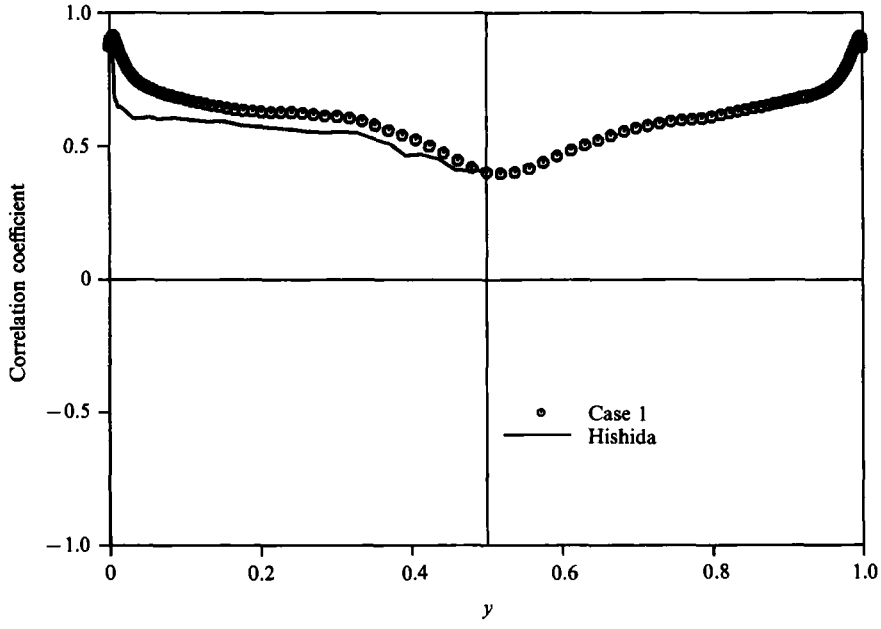

FIGURE 5. Correlation coefficient between the GS streamwise component fluctuations and the GS scalar fluctuations from Case 1 in comparison to the experimental data of Hishida *et al.* (1986).

the velocity and scalar profiles predicted for a linear sublayer, and both show an expected agreement. In Case 2, a significant deviation from the logarithmic profile exists in the central region of the channel, with Nakajima *et al.* (1980) and Tsai *et al.* (1987) obtaining similar results. When the cross-term models for τ_{ij} and τ_j^θ are not included in the LES computation, the von Kármán constant for the obtained mean

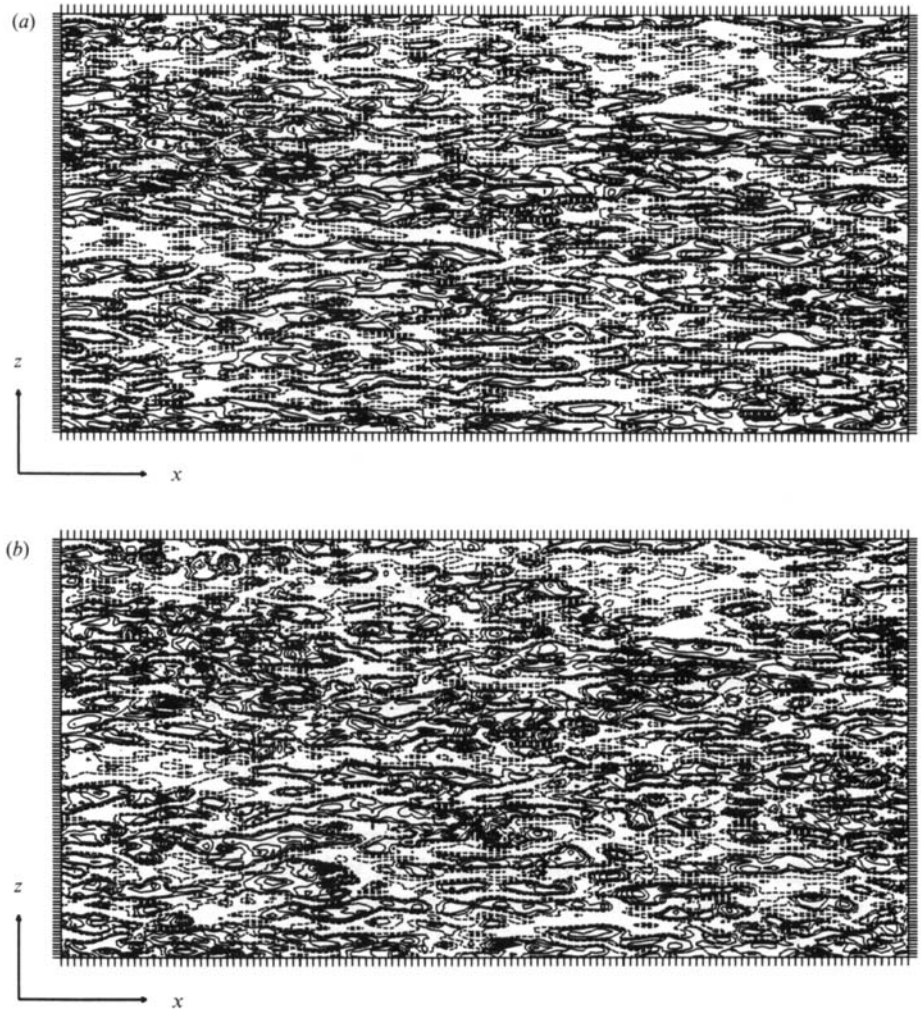

FIGURE 6. (*a*) Contour lines of $\bar{u}''$ in the (x, z)-plane at $y_+ = 8.7$ from Case 1. The hatch marks in the figure represent grid point distributions. (*b*) Contour lines of $\bar{\theta}''$ in the (x, z)-plane at $y_+ = 8.7$ from Case 1. The hatch marks in the figure represent grid point distributions.

scalar profile was 0.58, being too high when compared to experimental measurements (Gibson *et al.* 1982; Nagano & Hishida 1985). Contrastingly, when these models were included, the constant decreased to 0.46, considerably closer in agreement with experimental measurements. Figure 4 shows the normal components of scalar fluxes from Case 1, and it can be seen that the total scalar flux balances the volumetrical scalar source term which is uniformly distributed inside the channel. The correlation coefficient of the streamwise component of the GS velocity ($\bar{u}''$) and GS scalar ($\bar{\theta}''$) fluctuations from Case 1 is shown in figure 5, where the cross-term contributions are included in this calculation. The scalar field has a remarkably high correlation with the velocity field component, and this is confirmed in figure 6 (*a*, *b*) by the streamwise velocity and scalar fluctuation contours in the (x, z)-plane. In figure 6 (*b*) the scalar field is similar to the streamwise velocity field, and both fields have the same streaky structure as that obtained by Kim (1988), thus depicting the flow process similarity between the dynamic and scalar fields. The correlation coefficient of GS normal

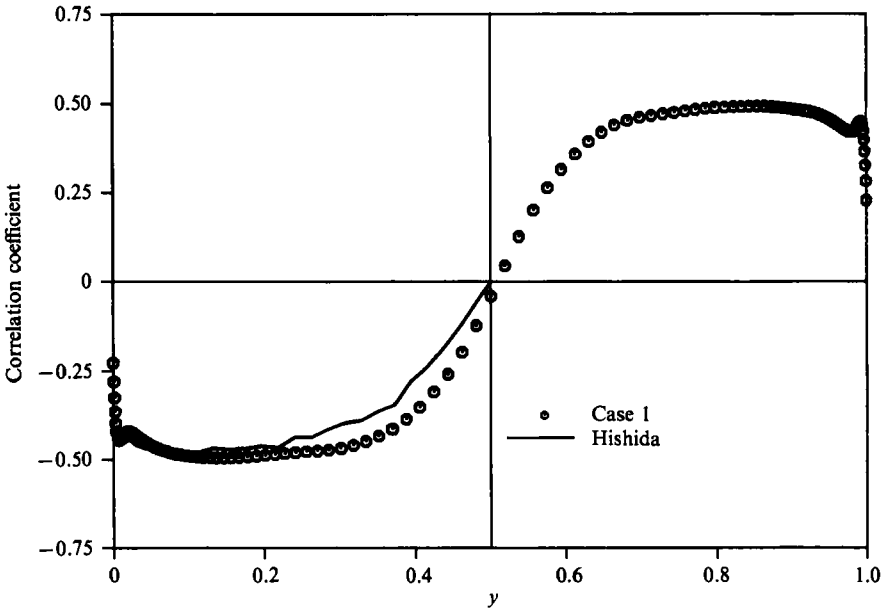

FIGURE 7. Correlation coefficient between the GS normal component fluctuations and the GS scalar fluctuations from Case 1 in comparison to the experimental data of Hishida *et al.* (1986).

velocity ($\overline{v}$) and the GS scalar fluctuation ($\overline{\theta}''$) from Case 1 is shown in figure 7. Figures 5 and 7 include the experimental measurements of Hishida *et al.* (1986), and are in overall agreement with these measurements except for the streamwise scalar flux correlation coefficient near the wall region which is believed to be caused by the difference in the Reynolds number used in the simulation and experiment. Figure 8(*a*) shows the streamwise two-point correlation function

$$R_{ii}(r_1; y) = \langle \overline{u}_i''(x+r_1, y, z)\, \overline{u}_i''(x, y, z)\rangle / \langle \overline{u}_i''^2(x, y, z)\rangle,$$

at $y = 0.0135$ ($y_+ = 17.3$). The observed correlation continues over a long distance in the downstream direction, and agrees with experimental results which indicate that the mean streamwise length of the streaks is greater than 1000 wall units (Blackwelder & Eckelmann 1979). Although the streamwise correlation has a non-zero value at a large separation, the value is very small, thereby implying that the computational results have not been significantly distorted by using the periodic boundary condition in the streamwise direction. To check the dependence of these streamwise correlations on the size of the computational box in the streamwise direction (L_x), L_x was increased to $4.8\,H$ in Horiuti (1987), and these results showed similar tendencies to Case 1. The spanwise two-point correlation functions $R_{ii}(r_3; y)$ defined by

$$R_{ii}(r_3; y) = \langle \overline{u}_i''(x, y, z)\, \overline{u}_i''(x, y, z+r_3)\rangle / \langle \overline{u}_i''^2(x, y, z)\rangle,$$

(located at the same position as in figure 8*a*), are shown in figure 8(*b*). There is no negative peak in $R_{11}(r_3; y)$ near $r_3 = 0$ as found in Horiuti (1987), hence the mean streak spacing was estimated as ≈ 140 (figure 6*a*) by using the position of the first negative peak of $R_{22}(r_3; y)$ in figure 8(*b*), and being close to the generally accepted value of 100 (Kline *et al.* 1967). The mean spacing of streaks from Case 3 was

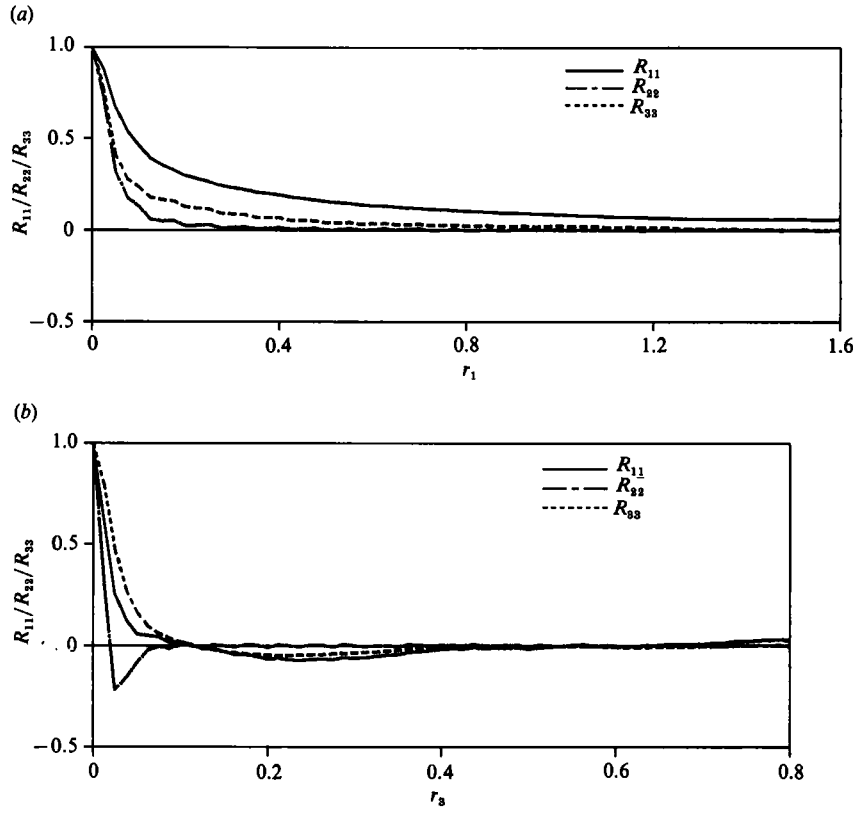

FIGURE 8. (*a*) Streamwise two-point correlation function $R_{ii}(r_1; y)$ from Case 1. (*b*) Spanwise two-point correlation function $R_{ii}(r_3; y)$ from Case 1.

approximately 240, thus a considerable improvement was obtained in Case 1. The use of the periodic boundary condition and the computational box length in the spanwise direction are subsequently concluded to be adequate.

3. Passive-scalar diffusion two-equation model

The two-equation model uses scalar variance (k_θ) and dissipation rate of scalar variance (ϵ_θ) as representative variables,

$$k_\theta = \langle \theta'^2 \rangle, \quad \epsilon_\theta = 2\left\langle \kappa \left(\frac{\partial \theta'}{\partial x_i}\right)^2 \right\rangle, \tag{11}$$

where θ' is a fluctuating scalar. The equations for the mean scalar Θ, k_θ and ϵ_θ become in plane channel flow,

$$\frac{\partial \Theta}{\partial t} = -\frac{\partial}{\partial y}\langle u_2' \theta' \rangle + \kappa \frac{\partial^2 \Theta}{\partial y^2}, \tag{12a}$$

$$\frac{\partial k_\theta}{\partial t} = -2\langle u_2' \theta' \rangle \frac{\partial \Theta}{\partial y} - \epsilon_\theta + D_{k\theta}, \tag{12b}$$

$$\frac{\partial \epsilon_\theta}{\partial t} = -C_{P1}\frac{\epsilon_\theta}{k_\theta}\langle u_2' \theta' \rangle \frac{\partial \Theta}{\partial y} - C_{P2}\frac{\epsilon_\theta}{k}\langle u_1' u_2' \rangle \frac{\partial U}{\partial y} - C_{D1}\frac{\epsilon_\theta^2}{k_\theta} - C_{D2}\frac{\epsilon \epsilon_\theta}{k} + D_{\epsilon\theta}, \tag{12c}$$

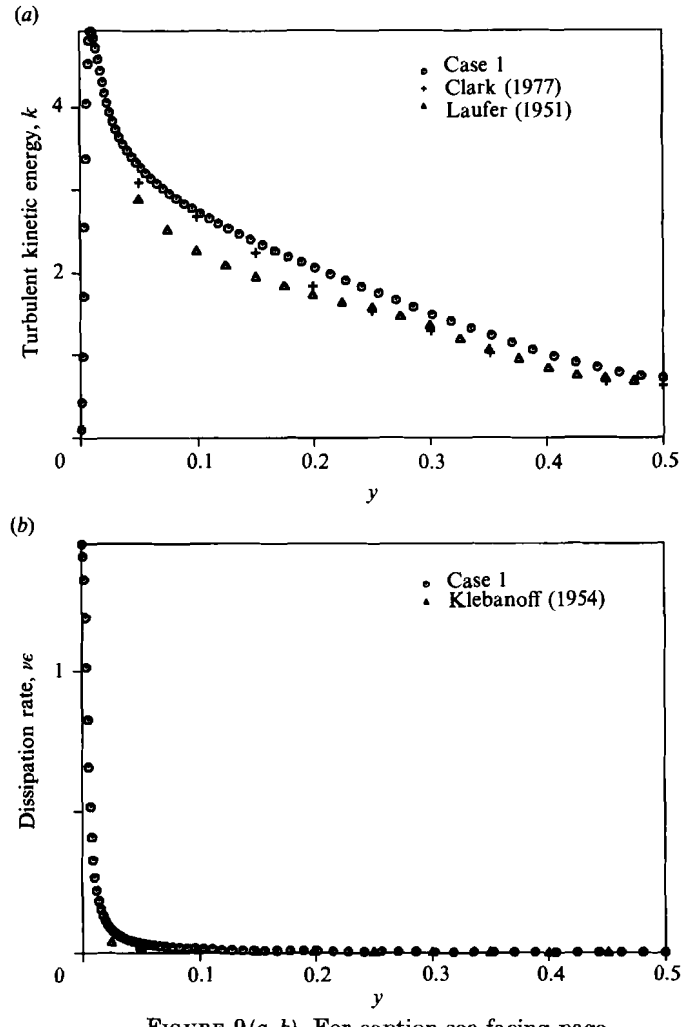

FIGURE 9(a, b). For caption see facing page.

where u_i' denotes the ith component of fluctuating velocity, and $D_{k\theta}$ and $D_{\epsilon\theta}$ are respectively the diffusion terms for the k_θ and ϵ_θ equations. These equations are then combined with the conventional $k-\epsilon$ models for velocity fields (NK 1988).

From the LES database described in §2, the quantities involved in the two-equation model were taken to be

$$U = \langle \bar{u} \rangle, \quad \Theta = \langle \bar{\theta} \rangle, \tag{13a, b}$$

$$\langle u_i' u_j' \rangle = \langle \bar{u}_i'' \bar{u}_j'' + (\bar{u}_i \bar{u}_j - \bar{\bar{u}}_i \bar{\bar{u}}_j) \rangle, \tag{13c}$$

$$k = \tfrac{1}{2}(\langle \bar{u}_i''^2 \rangle + \langle \bar{u}_i^2 - \bar{\bar{u}}_i^2 \rangle), \tag{13d}$$

$$\epsilon = \left\langle \nu_e^{\mathrm{LES}} \left(\frac{\partial \bar{u}_i}{\partial x_j} + \frac{\partial \bar{u}_j}{\partial x_i} \right)^2 + \nu \left(\frac{\partial \bar{u}_i}{\partial x_j} \right)^2 \right\rangle + (\text{Leonard \& Bardina terms}), \tag{13e}$$

$$k_\theta = \langle \bar{\theta}''^2 + (\bar{\theta}^2 - \bar{\bar{\theta}}^2) \rangle, \tag{13f}$$

$$\epsilon_\theta = 2 \left\langle (\kappa_e^{\mathrm{LES}} + \kappa) \left(\frac{\partial \bar{\theta}}{\partial x_i} \right)^2 \right\rangle + 2 \text{ (Leonard \& Bardina terms)}, \tag{13g}$$

$$\langle u_i' \theta' \rangle = \langle \bar{u}_i'' \bar{\theta}'' + (\bar{u}_i \bar{\theta} - \bar{\bar{u}}_i \bar{\bar{\theta}}) \rangle, \tag{13h}$$

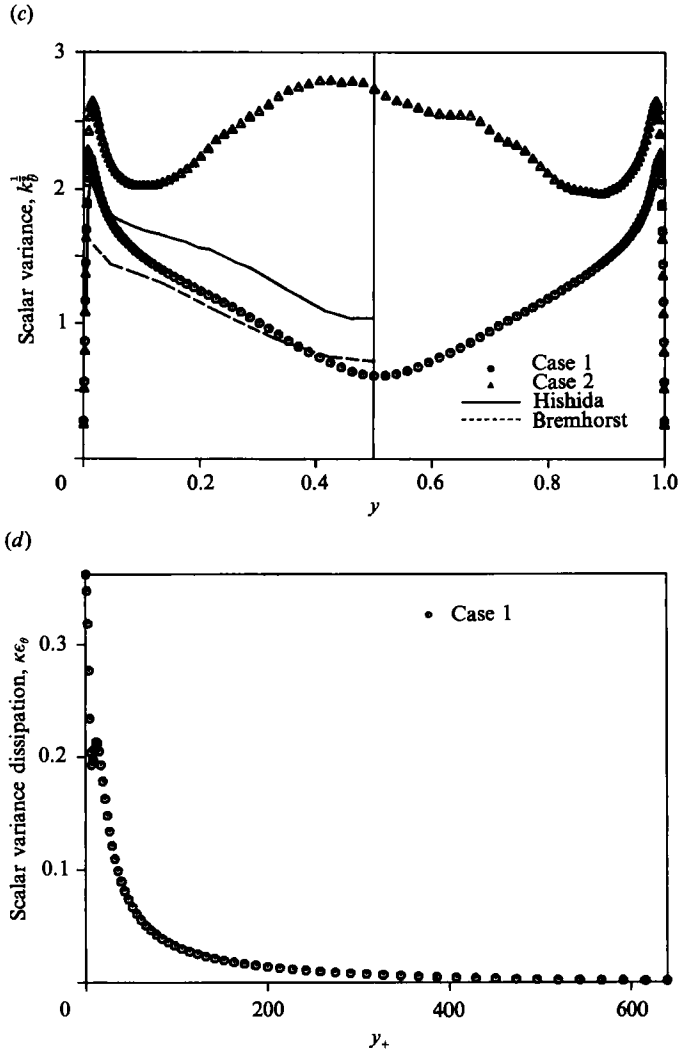

FIGURE 9. (*a*) Distribution of turbulent kinetic energy (k) from Case 1. (*b*) Distribution of dissipation rate of k (ϵ) from Case 1. (*c*) Distribution of scalar variance root values ($k_\theta^{\frac{1}{2}}$). Computational data from Cases 1 and 2, experimental data of Hishida *et al.* (1986), experimental data of Bremhorst *et al.* (1970). (*d*) Distribution of dissipation rate of k_θ (ϵ_θ) from Case 1 are shown.

where SGS contributions are not included in the evaluation of $\langle u_i' u_j' \rangle$, k, $\langle u_i' \theta' \rangle$, k_θ. The magnitude of the SGS turbulent energy and the SGS scalar fluctuations cannot be determined directly in the Smagorinsky model because one numerical constant which is independent of the Smagorinsky constant (C_S) must be properly chosen (Horiuti 1985), and it appears there is no systematic way to determine it using this model. The profiles of k, ϵ, $k_\theta^{\frac{1}{2}}$, ϵ_θ are shown in figure 9(*a–d*), and the correlation of k (figure 9*a*) and ϵ (figure 9*b*) with experimental measurements is good. The data for k from Laufer (1951) is slightly less than other data, and $k_\theta^{\frac{1}{2}}$ from Case 1 shows agreement near the wall with the experimental measurement of Hishida *et al.* (1986), although the computational data is smaller in the channel's central region (figure 9*c*). When compared to the experimental data of Bremhorst & Bullock (1970), the computational data is greater near the wall, while showing good agreement near the

channel centre. Grötzbach & Schumann (1979) investigated on the two-part model for the SGS scalar fluxes in plane channel flow, with the scalar being similarly input as in Case 1. Artificial boundary conditions designed to be consistent with the law of the wall were used to simulate the inner layer of the channel. The SGS scalar fluxes were split into a locally isotropic and inhomogeneous parts, i.e.

$$-\overline{u_i^{\mathrm{SGS}}\theta^{\mathrm{SGS}}} = \kappa_e^{\mathrm{H}}\frac{\partial}{\partial x_i}(\bar{\theta}-\langle\bar{\theta}\rangle)+\kappa_e^{\mathrm{I}}\frac{\partial}{\partial x_i}\langle\bar{\theta}\rangle, \tag{14}$$

where the different eddy diffusivities $\kappa_e^{\mathrm{H}}/\kappa_e^{\mathrm{I}}$ were used for the isotropic/inhomogeneous parts. When the inhomogeneous part was neglected, higher scalar variances resulted, i.e. when the two-part model was not employed the maximum value of $k_\theta^{\frac{1}{2}}$ was ≈ 2.7, whereas if the two-part model was used it was ≈ 2.0. The use of the two-part model had no effect in the region away from the wall because no appreciable differences were found. The peak value of $k_\theta^{\frac{1}{2}}$ in Case 1 is approximately 2.2, and is not significantly larger than either the experimental measurements by Hishida *et al.* (1986) or the numerical data by Grötzbach & Schumann (1979), thus when considering the uncertainties in the experimental measurements, the Case 1 computational data appears to be in good agreement with these measurements. The correlation coefficients of scalar fluxes are also in good agreement with the experimental measurements (figures 5 and 7), implying these scalar fluxes are well reproduced, and therefore leading to the two-part model not being used here. Furthermore, the mean scalar gradient of the two-part model directly influences the evaluation of SGS scalar fluxes, although this is surprising since the SGS scalar fluxes must be determined locally (Horiuti 1987). A significant difference in k_θ near the wall in Grötzbach & Schumann (1979) may be attributed to their artificial boundary condition. The distribution of $k_\theta^{\frac{1}{2}}$ from Case 2 is included in figure 9(*c*), where the slight asymmetry of scalar fluctuations around the centreline of the channel possibly indicates that the total averaging time in Case 2 is marginally sufficient. The magnitude of $k_\theta^{\frac{1}{2}}$ is close to that of Case 1 near the wall, whereas it is much larger in the central region of the channel. Since a mean scalar gradient is present in the channel central region in Case 2 (figure 3), scalar fluctuations occur there in contrast to Case 1. Nakajima *et al.* (1980) experiments measured similar distribution of scalar fluctuations (figure 9*c*), and Tsai *et al.* (1987) reproduced the same mean results by LES.

The NK (1988)/Yoshizawa (1988) model solves (12*a*)–(12*c*) with the aid of an eddy diffusivity concept, modelling the scalar fluxes as

$$-\langle u_i'\theta'\rangle = \kappa_e\frac{\partial\Theta}{\partial x_i}+\kappa_{etj}^{A}\frac{\partial\Theta}{\partial x_j}. \tag{15}$$

The first right-hand side term represents conventional isotropic eddy diffusivity (κ_e), whereas the second represents anisotropy of scalar fluxes. The profiles of turbulent Prandtl number (Pr_t) from Cases 1 and 5, defined by $Pr_t = \nu_e/\kappa_e$, are shown in figure 10, where eddy viscosity ν_e is defined as

$$\langle u_1'u_2'\rangle = -\nu_e\frac{\partial U}{\partial x_2}. \tag{16}$$

To provide a comparison, the experimental measurements by Hishida *et al.* (1986), the computational data obtained by Nagano, Tagawa & Niimi (1988) using the two-equation model, and the RANS computational data using an empirical Pr_t formula

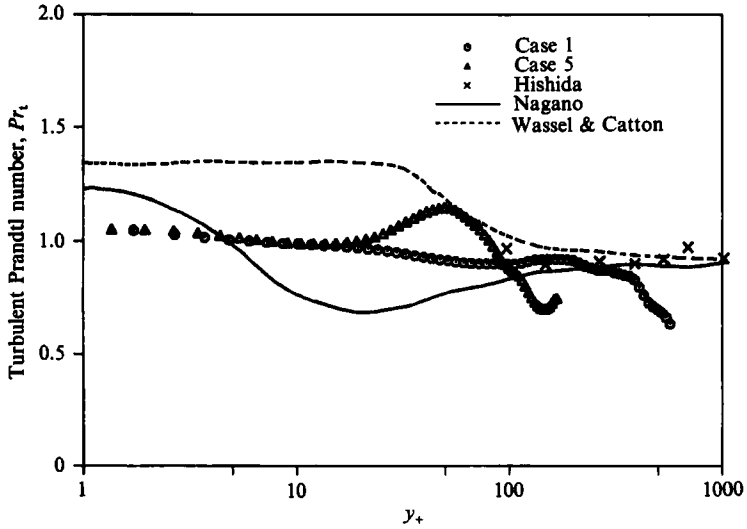

FIGURE 10. Profiles of turbulent Prandtl number Pr_t. Computational data from Cases 1 and 5, experimental data of Hishida *et al.* (1985), computational data of Nagano *et al.* (1988), and computational data of Wassel & Catton (1973) are shown.

by Wassel & Catton (1973) are included. The Pr_t profile from Case 1 is in fairly good agreement with Hishida *et al.* (1986), except in the channel central region. The profile from Case 5 correlates well with Case 1 in the wall vicinity, however, it overshoots at $y_+ \sim 50$ and gradually approaches ≈ 0.7, having a similar distribution to the one found in the DNS data of Kim (1988). Using these results it is concluded that the reliability of LES/DNS databases is acceptable, thus model validation was conducted using the presented databases.

In both NK (1988) and Yoshizawa (1988), κ_e is expressed as

$$\kappa_e = C_\kappa \frac{k^2}{\epsilon} r^p, \tag{17}$$

where r is the ratio of the velocity dissipation to the scalar dissipation timescales,

$$r = \frac{k}{\epsilon} \Big/ \frac{k_\theta}{\epsilon_\theta}. \tag{18}$$

By solving the transport equations for k, ϵ, k_θ and ϵ_θ, and incorporating the representative variable r into the eddy diffusivity, the use of *ad hoc* assumptions for the turbulent Prandtl number Pr_t can be avoided, while also including Prandtl number dependence. The importance of r in scalar diffusion is known, e.g. Elgobashi & Launder (1983). In NK (1988), p was chosen as $-\frac{1}{2}$ based on both experimental measurements (Hishida *et al.* 1986) and the assumption that the appropriate scalar fluctuation timescale is an arithmetic mean of the dynamic and scalar timescales. Yoshizawa (1988) derived the exponent based on a direct interaction approximation (DIA) approach combined with scale parameter expansions.

Leslie (1973) and Yoshizawa (1988) modelled anisotropic representation coefficient of scalar fluxes as

$$\kappa^A_{etj} = -C^A_\kappa \frac{k^3}{\epsilon^2} r^{p-1} \frac{\partial U_i}{\partial x_j}, \tag{19}$$

where C_κ^A is a constant. Yoshizawa (1988) set $p = -2$ for (17). The terms in (19) are generated by the second-order terms in the scale parameter expansion (Yoshizawa 1985), i.e. in the expansion products of the first-order velocity and scalar fluctuation terms. When (19) and (15) are combined in plane channel flow, only the second term remains for the streamwise component of scalar fluxes, while the first term remains for the normal component.

4. Model assessment

The two-equation model is assessed using the eddy diffusivity κ_e. Figure 11(*a*) shows four Case 1 eddy diffusivity profiles obtained from the LES database using (15), and for (17) with $p = -\frac{1}{2}$, $p = -2$, and $p = 0.9$, where quantities contained in the models were computed using the LES database of Case 1. In (17) the numerical constant C_k and p are optimized using a least-squares fitting method, being simultaneously optimized at 0.9 and 0.055, respectively, and at optimization $C_\kappa = 0.089$ ($p = -\frac{1}{2}$) and $C_\kappa = 0.15$ ($p = -2$). A least-squares fitting was performed which excluded the wall vicinity and the central region of the channel. This was done in the wall region because the damping functions in the two-equation model are important (§5), and the central region is also excluded because the departure from the logarithmic law is significant, turbulence is intermittent, and in the energy budget of Type I the diffusion terms are balanced by the dissipation terms. Hence the models of the diffusion terms are more important, and it is not necessary to evaluate the eddy diffusivity models in this region. Contrary to previous reports, p was found to be positive, and models using $p = -\frac{1}{2}$ or -2 are quite inaccurate in the region where κ_e appreciably changes ($y_+ = 100 \sim 200$) (figure 11*a*). When $p = -2$, a noticeably poor correlation occurs with the LES data with this region coinciding with the region where the timescale ratio r has large variations. Even though Yoshizawa (1988) demonstrated that his model for normal components of scalar fluxes had good agreement with the experimental measurements by Tavoularis & Corrsin (1981), the variation of r in these experiments was negligibly small. It is therefore felt that a fair evaluation of p must be done in flow regions where r changes substantially, because if the variation of r is negligibly small, the magnitude of the eddy diffusivity can be compensated for by adjusting the proportional coefficient in (17) C_κ. To determine dependence of p on the grid resolution in LES, the same evaluation was made in figure 11(*b*) for Case 3, with the resulting optimized p and C_κ respectively being 0.5 and 0.05 ($C_\kappa = 0.071$ ($p = -\frac{1}{2}$) and $C_\kappa = 0.11$ ($p = -2$)). There is no guarantee that these numerical results have not been distorted by the turbulence models incorporated into LES, thus the eddy diffusivities for Case 5 were obtained as shown in figure 11(*c*). The optimized p/C_κ were 2.4/0.015 ($C_\kappa = 0.054$ ($p = -\frac{1}{2}$) and $C_\kappa = 0.125$ ($p = -2$)). Cases 3 and 5 gave similar mean results as in Case 1, with a low correlation being found between the models using $p = -2$ or $-\frac{1}{2}$ and the numerical databases. Until now, the evaluation of p has been made using the normal scalar flux, although it may also be done via the streamwise scalar AR flux:

$$\langle u_1' \theta' \rangle = C_\kappa^A \frac{k^3}{\epsilon^2} r^{p-1} \frac{\partial U}{\partial y} \frac{\partial \Theta}{\partial y}. \tag{20}$$

Using (20) the best fit with the LES data was obtained in Case 1 with $p \approx +1$. In Yoshizawa (1988) the overall agreement of $\langle u_1' \theta' \rangle$ with the experimental measurements by Tavoularis & Corrsin (1981) was demonstrated with $p = -2$,

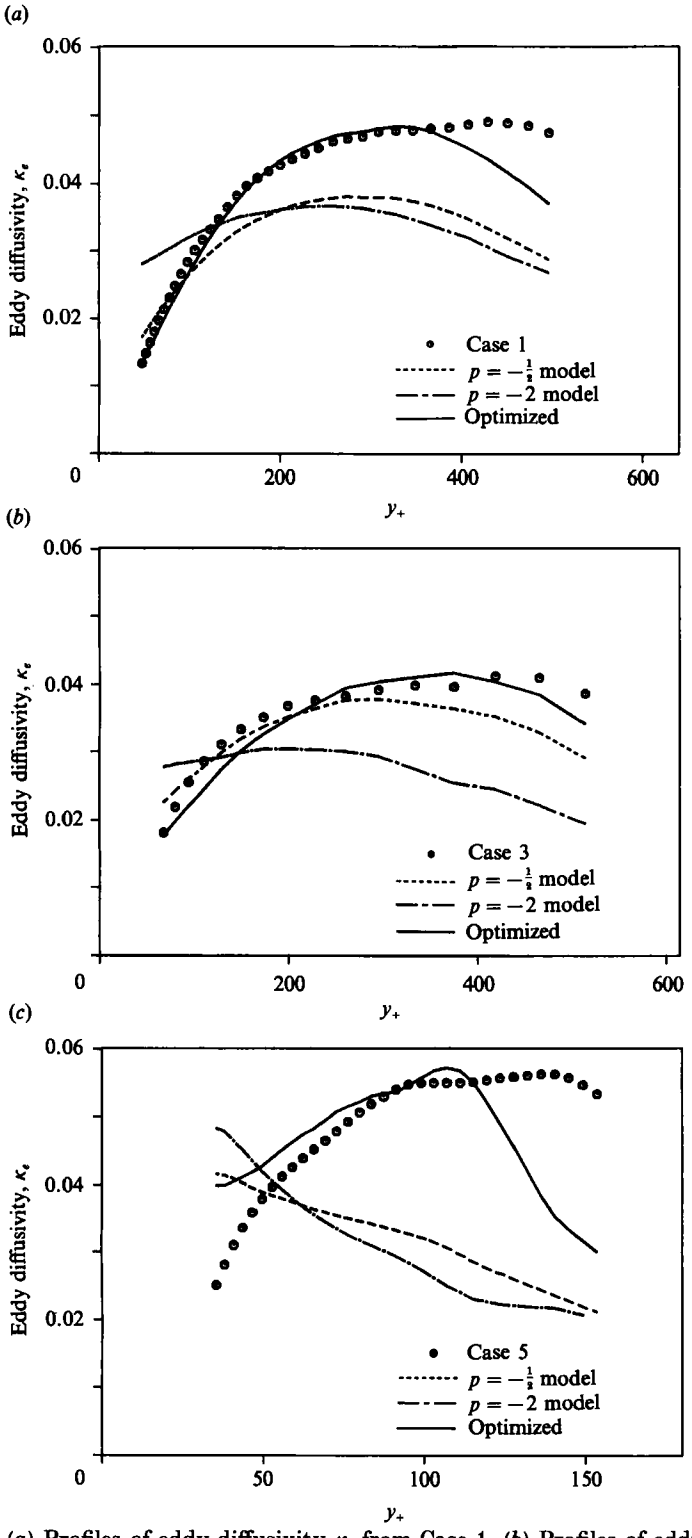

FIGURE 11. (*a*) Profiles of eddy diffusivity κ_e from Case 1. (*b*) Profiles of eddy diffusivity κ_e from Case 3. (*c*) Profiles of eddy diffusivity κ_e from Case 5.

however, a deviation occurred from the experimental measurements ($x/h \sim 7.5$ in figure 2, Yoshizawa 1988). This model's marginal accuracy is also evident in the numerical results by Nagano *et al.* (1988), where the data was obtained by incorporating the equation (17) model ($p = -2$) into the actual two-equation model computation. The distribution of Pr_t in figure 10 shows a large dip near the wall, being absent from other results. The dependence of model performance on the method to input the scalar source is examined in Cases 2 and 4, with the eddy diffusivities from Case 2 shown in figure 12, thereby confirming the reduced performance of the $p = -\frac{1}{2}$ or -2 models with the LES data. The optimized p value in Case 2 was 3.0 with $C_\kappa = 0.08$ ($C_\kappa = 0.11$ ($p = -\frac{1}{2}$) and $C_\kappa = 0.17$ ($p = -2$)), and was similar to the Case 4 mean value. It is concluded that selecting $p = 1 \sim 3$ yields a much higher correlation with the LES/DNS databases, further noting that this conclusion is supported by Kasagi (private communication), who used plane channel flow DNS which utilized a different method to input the scalar source.

Nagano *et al.* (1988) pointed out that p should approach -2 in the near-wall vicinity in order to achieve a correct limiting wall behaviour of scalar fluxes when the scalar is input in the same manner as in Types I and II, and accordingly revised the model to set p equal to -2. Since the statistical theory of Yoshizawa (1988) is invalid near the wall, the coincidence of the values determined by statistical theory and wall behaviour is rather accidental, and thus there is no definite reason to select a p that is away from the wall equal to one in the wall's near vicinity. In order to apply the two-equation models to the simulations of passive-scalar diffusion which are accurate up to the wall, an eddy-diffusivity model with a correct wall-limiting behaviour is desirable. In heat transfer problems, it is well known that unless the correct wall-limiting behaviour is satisfied, the model provides inaccurate numerical results (Myong 1988). Subsequently, an eddy-diffusivity model which accounts for a smooth bridging between the two extreme cases of $p \sim 1$ and $p = -2$ must be developed. Furthermore, when the equation (17) model with $p = 1.0$ is incorporated into an actual computation, it was found that the computation is unstable, believed to be the result of a substantially smaller magnitude of eddy diffusivity in the central region of the channel. To counter these drawbacks, a modification is made on the eddy diffusivity within the framework of Yoshizawa (1985), being represented as

$$\kappa_e = C_1 \int_{k_M}^{\infty} \tilde{k}^2 \frac{\sigma(\tilde{k})}{\omega(\tilde{k}) + \omega_\theta(\tilde{k})} \mathrm{d}\tilde{k}, \tag{21}$$

where $\tilde{k}$ denotes the wavenumber, ω the reciprocal of the response timescale of the velocity field, ω_θ the reciprocal of the response timescale of the scalar field, σ the modal energy, k_M is a cutoff wavenumber $2\pi/l_\theta$ (l_θ is the characteristic scalar length), and C_1 is a model constant. The determinations of σ, l_θ, and ω_θ adopted in Yoshizawa (1985) are not fixed, enabling several modifications, i.e. an intermittency factor may be incorporated into the modal energy, or the cutoff wavenumber may be given by blending the characteristic lengthscales for the velocity and scalar fields. These modifications resulted in slightly changing p. It should be noted that the optimized p values varied for Cases 1–5 ($p = 0.5 \sim 3$), although all Cases clearly show that these values are positive in contrast to the negative values obtained in the previous models. The cause of these variations has not been clarified, but they may be related to either the intermittency factor in modal energy or the characteristic lengthscale, i.e. the intermittency factor which represents the turbulent eddy or coherent structure may be dependent on both the method in which the passive scalar field is

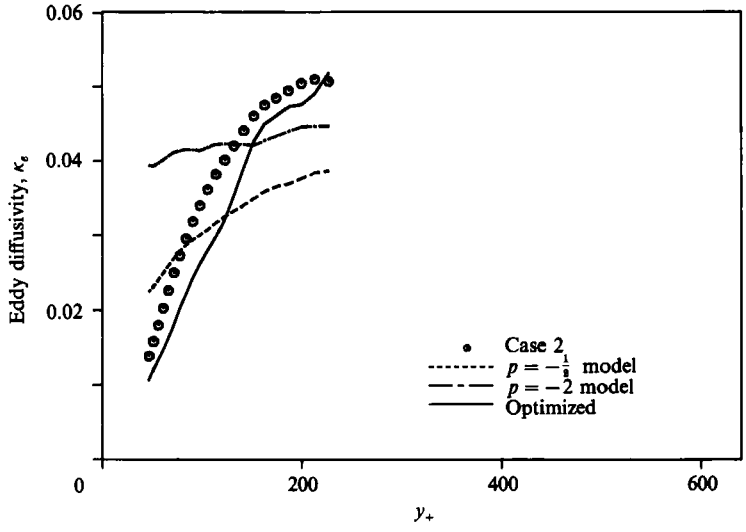

FIGURE 12. Profiles of eddy diffusivity κ_e from Case 2.

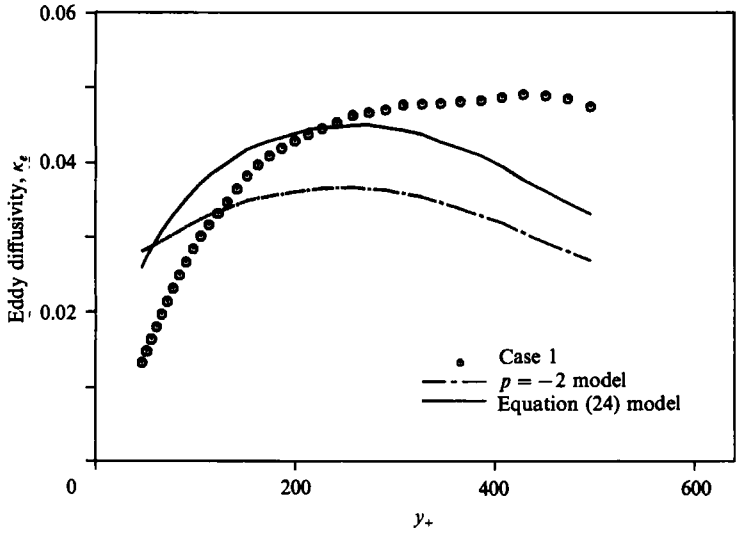

FIGURE 13. Profiles of eddy diffusivity κ_e from Case 1.

driven and also the Reynolds number. When the scalar field boundary condition was the same, the p values were close (0.9 (Case 1) and 0.5 (Case 3) for Type I, and 3.0 (Cases 2 and 4) for Type II), being slightly larger (2.4) when a low Reynolds number was used for Type I (Case 5). It appears that a systematic method to include the intermittency factor has not yet been developed, and thus this will be left to future work. It was found, however, that κ_e was essentially unaffected in the channel central region by incorporating the intermittency factor into the modal energy, i.e. the magnitude of κ_e remained substantially small as shown in figure 11. The modification adopted here lets ω_θ be dependent on the ratio r of the timescales. In Yoshizawa (1979), a proportional relationship between ω and ω_θ is used, where a constant coefficient g is assumed,

$$\omega_\theta = g\omega, \quad \omega = C_2 \epsilon^{\frac{1}{3}} \tilde{k}^{\frac{2}{3}}, \tag{22}$$

where C_2 is a model constant. In the present study ω_θ is redefined as

$$\omega_\theta = C_\alpha r^\alpha \omega, \tag{23}$$

where C_α is a model constant. When (23) is substituted into (21), κ_e is obtained,

$$\kappa_e = C_\kappa \frac{k^2}{\epsilon} r^{-2} \frac{1}{1+C_\alpha r^\alpha}. \tag{24}$$

To make it easier to develop a model having the correct limiting wall behaviour, in (24) p is set equal to -2. When α is set to -3, the r exponent in κ_e effectively becomes 1 when r is small, and -2 when r is large, providing a smooth bridging between these two exponents. Equation (24) was tested by comparing it with the LES data from Case 1 as shown in figure 13, where C_κ, C_α, and α are respectively chosen as 0.22, 0.5 and -4. As a comparison, the distribution of eddy diffusivity for the $p = -2$ model (figure 11*a*) is shown in figure 13. In the region $y_+ = 100 \sim 200$, the poor correlation of this model is significantly improved, and also the instability found when using the $p = +1$ model was prevented.

5. Algebraic scalar flux model comparison

Rogers *et al.* (1989 hereinafter referred to as RMR) thoroughly investigated the algebraic model for passive-scalar diffusion of Gibson & Launder (1976) using the DNS databases for homogeneous shear and channel flows, and reported an approximate alignment of the sum of the pressure–scalar gradient and velocity gradient–scalar gradient terms with the scalar flux vector itself. By combining the alignment of the time derivative terms with the scalar flux vector, RMR simplified the algebraic scalar flux model (AFM). In plane channel flow, their model becomes

$$\langle u_1' \theta' \rangle = C_D \frac{k}{\epsilon} \langle u_1' u_2' \rangle \frac{\partial \Theta}{\partial y} - \frac{1}{C_D^2} \frac{k^2}{\epsilon^2} \langle u_2'^2 \rangle \frac{\partial U}{\partial y} \frac{\partial \Theta}{\partial y}, \tag{25a}$$

$$\langle u_2' \theta' \rangle = -\frac{1}{C_D} \frac{k}{\epsilon} \langle u_2'^2 \rangle \frac{\partial \Theta}{\partial y}, \tag{25b}$$

where C_D is a model constant which is introduced to represent a Prandtl number effect and the spatial variation of the timescale. By fitting (25) to the DNS data, RMR proposed

$$C_D = 18.0 \left(1 + \frac{130}{Pr\, Re_t}\right)^{0.25} \left(1 + \frac{12.5}{Re_t^{0.48}}\right)^{-2.08}, \tag{26}$$

where Re_t is the turbulent Reynolds number defined by $k^2/\nu\epsilon$. In both the presented and RMR models, the basic timescale adopted in the eddy diffusivity for the normal scalar flux is k/ϵ. The representative energy scale selected in (24) is k, whereas (25*b*) is used for the normal component of turbulence fluctuations. The correction in the timescale in (24) is

$$\frac{1}{r^2} \frac{1}{1+C_\alpha r^\alpha}, \tag{27}$$

whereas in RMR (1989) it was C_D. Notice that (26) and (27) are similar in functional form, although r is used in (27), whereas Re_t is used in (26). In addition, their asymptotic behaviour is different, i.e. when Re_t is very small, the effective Re_t

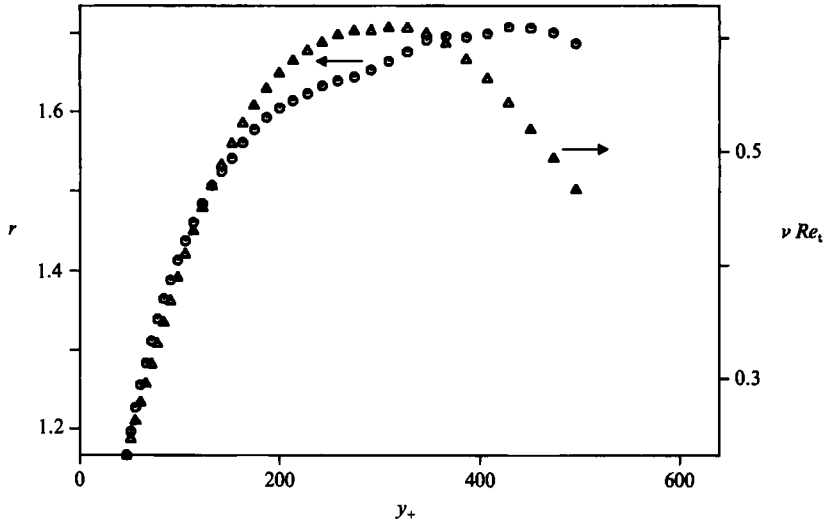

FIGURE 14. Profiles of timescale ratio r and turbulent Reynolds number Re_t from Case 1.

exponent in (26) becomes -0.748, and when Re_t is very large, C_D becomes 18.0. In (22) the constant g was set equal to 1.6 to be consistent with the response function equation in Yoshizawa (1979). By integrating the response equation with respect to time $(0 \rightarrow \infty)$, a constrained relation for ω and ω_θ was obtained which consistently solved the equations, and by numerically solving this relation equation, g was determined, although (23) may not always satisfy this consistency requirement. In order to avoid the infrared divergence of the response equation (Leslie 1973), a modified geometric function $c(k,p,q)$ was introduced by Yoshizawa (1978). The equation for the scalar response function was modified as in Yoshizawa (1979), and a value of $g = 1.6$ was selected based on this modified geometric function. The assumptions involved in deriving the modified geometric function and the uniqueness of the function, have not yet been clarified, thus it is believed that the introduction of g as a value other than 1.6 is possible. In practical applications, modifications as in (26) or (27) are necessary to explain real flow, but as RMR (1989) noted, basing C_D on r may violate the linearity and independence principles by Pope (1983). In the LES database for plane channel flow, however, it was found that the profile of r from Case 1 is very close to that of Re_t in the region $y_+ = 50 \sim 400$ (figure 14), with r being asymptotically equal to 1.7 near the channel central region. Beguier, Dekeyser & Launder (1978) estimated this ratio using experimental measurements in the boundary layer on a heated flat plate, in the pipe flow, and in the wake of a heated cylinder. It was found in all cases that the ratio is nearly uniform, being ≈ 2.0. The presented data is close to this estimate, although the slight downward trend of the distribution of r in Beguier *et al.* (1978) was not observed. The simulated Reynolds number may not be large enough to confirm this trend, but the similarity between r and Re_t implies that at this Prandtl number the final C_D value for plane channel flow does not strongly depend on either r or Re_t if the coefficients of (26) and (27) are properly selected. It was also revealed that the function C_D is closely related to (23) for the response timescale relation of velocity and scalar fields. The similarity between r and Re_t found here, however, may possibly depend on flow configurations since RMR (1989, p. 92) noted that for homogeneous shear flows, 'r rapidly approaches a constant value whereas C_D continually increases'. Tests of similarities

between these values will be performed in the future using a variety of other flows, thereby enabling its dependence on the Prandtl number to be further investigated. The Prandtl number dependence is empirically incorporated by implicitly including Pr in the RMR model, whereas it is represented by the dependence of r on Pr in NK (1988) and Yoshizawa (1988). The turbulent Reynolds number peaked at $y_+ \sim 350$ and decreased toward the channel centre (figure 14). A correction in the timescale in the eddy diffusivity should become asymptotically uniform near the central region of channel, yet when Re_t is chosen as the variable this does not occur, implying that Re_t may not be a feasible representative variable for the correction function in this region. When the Pope (1983) model was used, where linearity and independence principles were strictly adhered to, erroneous results were obtained, therefore the exclusion of r when defining C_D may lower the practical applicability of this model.

Anisotropic representation of the Reynolds stresses $\langle u_i' u_j' \rangle$

$$\begin{aligned}\langle u_i' u_j' \rangle = {} & \tfrac{2}{3}k\delta_{ij} - C_\nu \frac{k^2}{\epsilon}\left(\frac{\partial U_i}{\partial x_j} + \frac{\partial U_j}{\partial x_i}\right) \\ & - \left[\frac{1}{3}\frac{k^3}{\epsilon^2}\left\{(C_{r1}+C_{r3})\frac{\partial U_l}{\partial x_m} + C_{r2}\frac{\partial U_m}{\partial x_l}\right\}\frac{\partial U_l}{\partial x_m}\right]\delta_{ij} \\ & + \frac{k^3}{\epsilon^2}\left\{C_{r1}\frac{\partial U_i}{\partial x_l}\frac{\partial U_j}{\partial x_l} + \frac{C_{r2}}{2}\left(\frac{\partial U_i}{\partial x_l}\frac{\partial U_l}{\partial x_j} + \frac{\partial U_j}{\partial x_l}\frac{\partial U_l}{\partial x_i}\right) + C_{r3}\frac{\partial U_i}{\partial x_i}\frac{\partial U_l}{\partial x_j}\right\}, \quad (28)\end{aligned}$$

has been successfully used to give accurate predictions of anisotropic turbulence intensities, where C_{r1}, C_{r2} and C_{r3} are the model constants (Nisizima & Yoshizawa 1987; Speziale 1987; Rubinstein *et al.* 1990). By substituting (28) into (25a) the streamwise scalar flux $\langle u_1' \theta' \rangle$ in plane channel flow is obtained,

$$\langle u_1' \theta' \rangle = -\frac{1}{C_D}\left(C_\nu + \frac{1}{C_D}\frac{2}{3}\right)\frac{k^3}{\epsilon^2}\frac{\partial U}{\partial y}\frac{\partial \Theta}{\partial y} + \frac{1}{3}\frac{1}{C_D^2}(C_{r1}-2C_{r3})\frac{k^5}{\epsilon^4}\left(\frac{\partial U}{\partial y}\right)^3\frac{\partial \Theta}{\partial y}. \quad (29)$$

The first right-hand side term in (29) is the same as (20) except for the coefficient, thus a close relationship between anisotropic representation of scalar fluxes and AFM is apparent. If the two-equation model approach is used in place of more sophisticated algebraic models, the terms in (29) must be supplemented to express the anisotropy of scalar fluxes. Anisotropic representations in both (20) and the first term in (29) appears among second-order terms in the scale parameter expansions of Yoshizawa (1988), whereas the last term in (29) among fourth-order terms. Similarly, by inserting (28) into (25b), the normal scalar flux $\langle u_2' \theta' \rangle$ is

$$\langle u_2' \theta' \rangle = -\frac{1}{C_D}\frac{k}{\epsilon}\left\{\tfrac{2}{3}k - \tfrac{1}{3}(C_{r1}-2C_{r3})\frac{\kappa^3}{\epsilon^2}\left(\frac{\partial U}{\partial y}\right)^2\right\}\frac{\partial \Theta}{\partial y}, \quad (30)$$

where the coefficient $C_{r1}-2C_{r3}$ is usually positive (Horiuti 1990). The second term is an extra term incorporated into the eddy diffusivity, and appears in the third-order expansion terms in anisotropic representation. Higher-order expansion terms in anisotropic representation generate higher-order derivatives for the mean velocity and scalar, hence AFM can be characterized as a subset of these expansions, consisting of only first-order derivatives of mean velocity and scalar and their products. Incorporating higher-order differentials may not be practically feasible since this requires additional boundary conditions. The effect of the second term in (30) is shown in figure 15 for the normal scalar flux of Case 1. In NK (1988), the Van

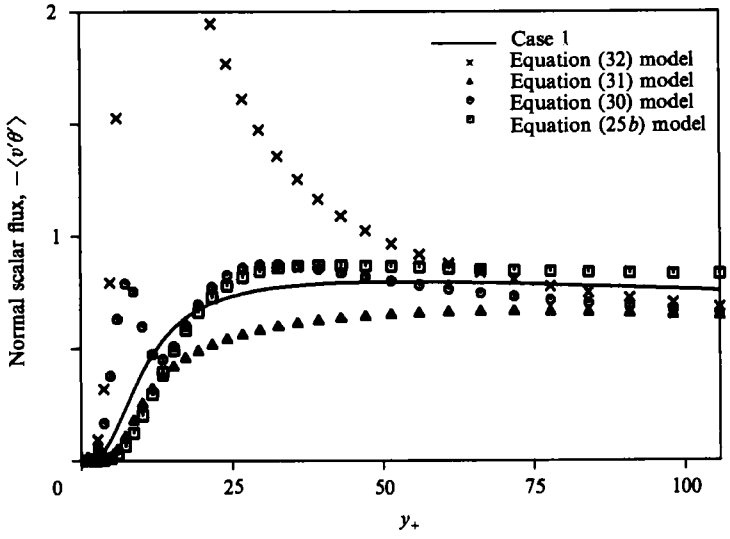

FIGURE 15. Distribution of mean scalar flux normal component $\langle u_2'\theta'\rangle$ in the vicinity of the lower wall. Shown are computational data from Case 1, equation (32) model with $C_\kappa = 0.089$, equation (31) model with $C_\kappa = 0.089$ and $A_+ = 30.5$, equation (30) model, and equation (25*b*) model.

Driest damping function (Van Driest 1956) was used to approximate the normal scalar flux combined with the eddy diffusivity of (17) ($p = -\frac{1}{2}$),

$$\langle u_2'\theta'\rangle = -C_\kappa \frac{k^2}{\epsilon} r^p (1-\exp(-y_+/A_+))^2 \frac{\partial \Theta}{\partial y}, \tag{31}$$

where C_κ is a model constant and A_+ was selected equal to 30.5. When the damping function was not multiplied, i.e. when using

$$\langle u_2'\theta'\rangle = -C_\kappa \frac{k^2}{\epsilon} r^p \frac{\partial \Theta}{\partial y} \quad (p = -\tfrac{1}{2}), \tag{32}$$

the flux profile showed a prohibitively large peak near the wall. The Van Driest damping function effectively suppressed this peak and gave a reasonably good correlation with the LES data. When third-order anisotropic representation of (30) was used, this large peak was suppressed as effectively as by the Van Driest damping function, except in close proximity to the wall, thereby indicating that third-order anisotropic representation may be used as an alternative method for empirical damping functions. In figure 15, C_D in (30) was set equal to 6.0, and $C_{r1} - 2C_{r3}$ was set equal to 0.016. The RMR model (equation (25*b*)) had good correlation with the LES data, although it was slightly higher at $y_+ \sim 25.0$. Therefore, without introducing an empirical damping function, the RMR model provides an effective reduction of the scalar flux near the wall, being mostly attributed to choosing the normal shear stress as the representative energy scale for eddy diffusivity. Since C_D in (26) does not affect this reduction, a more preferable energy scale for eddy diffusivity is the normal component of turbulent fluctuations rather than the total energy k. It should be noted that the evaluation of the RMR model in both the present study and in RMR (1989) was performed by inserting the normal shear stress profile obtained from LES/DNS databases into (25*b*). An accurate model to represent the normal shear stress must be provided for actual use of the model of (25*b*), whereas the presented model of (30) is self-contained with regard to the normal

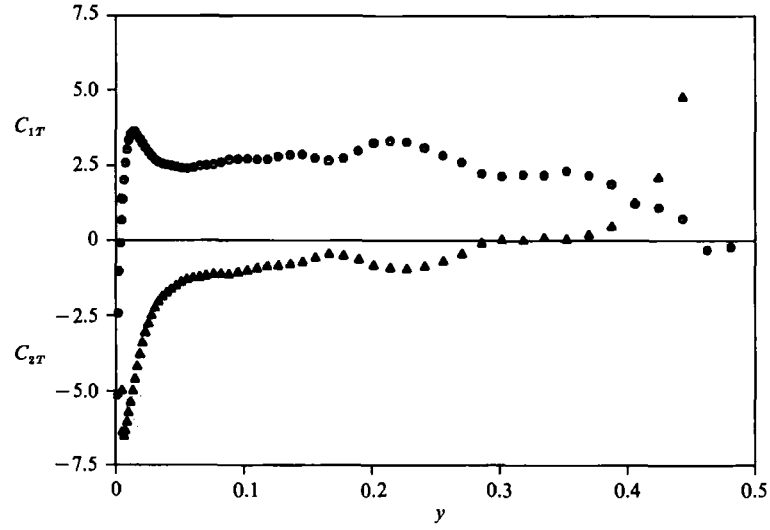

FIGURE 16. Distributions of model coefficients C_{1T} and C_{2T} obtained from (34) in Case 1.

shear stress. Both the NK (1988) model of (31) and the RMR model do not correctly satisfy the scalar flux wall-limiting behaviour, and in the future a two-equation model which combines (24) and (30) must be developed to account for this phenomenon.

A final comparison to RMR is conducted using the pressure–scalar gradient terms (Gibson & Launder 1976)

$$\left\langle p' \frac{\partial \theta'}{\partial x_i} \right\rangle = -C_{1T} \frac{\epsilon}{k} \langle \theta' u_i' \rangle + C_{2T} \langle \theta' u_j' \rangle \frac{\partial U_i}{\partial x_j}. \tag{33}$$

The first term in the right-hand side models the 'slow' part of pressure–scalar gradient terms, and the second right-hand side term models the 'rapid' part. RMR found that the pressure–scalar gradient term is approximately aligned with the scalar flux vector itself, i.e. C_{2T} was very small when the model of (33) was fitted to the DNS data. In plane channel flow, (33) becomes

$$\left\langle p' \frac{\partial \theta}{\partial x_1} \right\rangle = -C_{1T} \frac{\epsilon}{k} \langle \theta' u_1' \rangle + C_{2T} \langle \theta' u_2' \rangle \frac{\partial U}{\partial y}. \tag{34a}$$

$$\left\langle p' \frac{\partial \theta'}{\partial x_2} \right\rangle = -C_{1T} \frac{\epsilon}{k} \langle \theta' u_2' \rangle, \tag{34b}$$

The distributions of C_{1T} and C_{2T} obtained by solving (34a) and (34b) are shown in figure 16, where k, ϵ, U and the scalar fluxes and pressure–scalar gradient terms were obtained using the LES database of Case 1. The C_{2T} value is very small except in the vicinity of the wall and the channel centre, and therefore the finding of RMR (1989) is confirmed. When the velocity gradient–scalar gradient terms

$$-(\nu + \kappa) \left\langle \frac{\partial u_i'}{\partial x_j} \frac{\partial \theta'}{\partial x_j} \right\rangle \tag{35}$$

are included in the right-hand side of (34), the C_{1T} and C_{2T} distribution showed only a slight change from those in figure 16, except in the vicinity of the wall, thereby implying that the contribution of the velocity gradient–scalar gradient terms in (35)

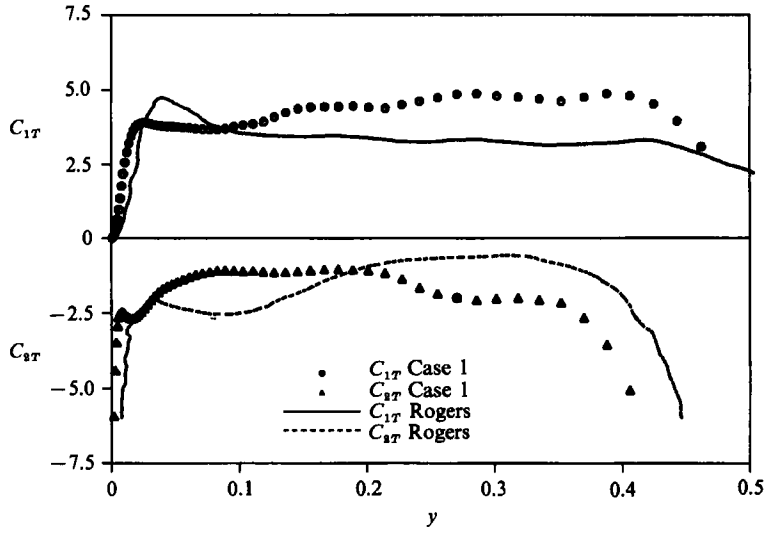

FIGURE 17. Distribution of C_{1T} and C_{2T} obtained from (37) in Case 1 and Rogers (private communication).

is confined to the vicinity of the wall. By neglecting diffusion terms (note that convection terms disappear in plane channel flow), the governing equations for scalar fluxes become

$$-\langle u_i' u_j' \rangle \frac{\partial \Theta}{\partial x_j} - \langle \theta' u_j' \rangle \frac{\partial U_i}{\partial x_j} + \left\langle p' \frac{\partial \theta'}{\partial x_i} \right\rangle = 0, \tag{36}$$

which provide alternative equations to determine C_{1T} and C_{2T},

$$\langle u_1' \theta' \rangle = -\frac{1}{C_{1T}} \frac{k}{\epsilon} \langle u_1' u_2' \rangle \frac{\partial \Theta}{\partial y} + (1 - C_{2T}) \frac{1}{C_{1T}^2} \frac{k^2}{\epsilon^2} \langle u_2'^2 \rangle \frac{\partial U}{\partial y} \frac{\partial \Theta}{\partial y}, \tag{37a}$$

$$\langle u_2' \theta' \rangle = -\frac{1}{C_{1T}} \frac{k}{\epsilon} \langle u_2'^2 \rangle \frac{\partial \Theta}{\partial y}. \tag{37b}$$

The C_{1T} and C_{2T} profiles from Case 1 obtained by solving (37*a*) and (37*b*) are shown in figure 17, with C_{1T} and C_{2T} being larger than in figure 16. An increase in the magnitude of C_{2T} is especially significant. Both C_{1T} and C_{2T} show an almost flat distribution throughout the channel, indicating that they may be modelled as a constant. Although C_{2T} shows a large deviation in the channel central region, it can still be modelled as a constant without causing a serious error because the magnitude of the scalar fluxes is small in this region. For comparison, the computational data by Rogers (private communication) using the DNS database for plane channel flow is included in figure 17, and in this data the Reynolds number was set at 360, similar to Case 5. In Launder (1975), C_{1T} was set at $2.5 \sim 5.0$ by fitting the model of (37) to the experimental measurements of Webster (1964), with the C_{1T} value in figures 16 and 17 being well within this range. On the other hand, C_{2T} is ≈ -1.0 in both the present study and Rogers (private communication), except in the proximity of the wall and the channel central region, whereas 0.5 has been commonly used following Launder (1975). Use of (37*a*) and (37*b*) results in a ratio of the streamwise to normal scalar flux of,

$$\frac{\langle u_1' \theta' \rangle}{\langle u_2' \theta' \rangle} = \frac{\langle u_1' u_2' \rangle}{\langle u_2'^2 \rangle} - \frac{1 - C_{2T}}{C_{1T}} \frac{k}{\epsilon} \frac{\partial U}{\partial y}. \tag{38}$$

Assuming equilibrium between the production and dissipation in the energy budget of the velocity field, (38) was rewritten by Launder (1975) as

$$\frac{\langle u_1' \theta' \rangle}{\langle u_2' \theta' \rangle} = \frac{\langle u_1' u_2' \rangle}{\langle u_2'^2 \rangle} + \frac{1 - C_{2T}}{C_{1T}} \frac{k}{\langle u_1' u_2' \rangle}. \tag{39}$$

Using the experimental data of Champagne, Harris & Corrsin (1970) for $\langle u_1' u_2' \rangle / \langle u_2'^2 \rangle$ and $k/\langle u_1' u_2' \rangle$, and Webster's scalar flux ratio data for homogeneous shear flow, Launder (1975) concluded that C_{2T} should be ≈ 0.5. The scalar flux ratio in Webster (1964) was approximately -1.1, whereas in the numerical data used here and in Rogers (private communication) the scalar flux ratio is approximately in the range -2.0 to -2.5, yielding $C_{2T} \approx -1.0$, and is in good agreement with the values in figure 17. An estimate of the positive C_{2T} values can be obtained from the lower estimated ratio of scalar fluxes in Launder (1975), thus C_{2T} is not believed to be a universal constant that is flow independent. It should be noted that in Launder (1975), the C_{2T} estimation error also comes from the equilibrium assumption, i.e. the ratio of the production to the dissipation term is not exactly equal to 1.0 (Rogers, private communication), and hence it is evident that the choice of $C_{2T} \approx -1.0$ is inconsistent with the RMR model of (25). In fact, the values of $\langle u_1' \theta' \rangle$ using this model are consistently smaller than the DNS data for plane channel flow in RMR (1989) (figures 12 and 13, RMR 1989). By setting $C_{2T} = -1.0$, the correlation to the DNS data can be significantly improved. When the diffusion terms were included in (37), C_{2T} was reduced somewhat, and if accurate models for the diffusion terms are provided, C_{2T} may be set to zero.

6. Summary and conclusions

A numerical assessment is made on the two-equation model for turbulent passive-scalar diffusion in plane channel flow using the databases derived from large-eddy and direct numerical simulations (LES/DNS), using up to 128^3 grid points. In LES, the scale similarity model (Bardina *et al.* 1980) was used for the cross-correlation terms in the filtered Navier–Stokes equations and the transport equations of passive scalar. The reliability of the databases was established by comparing them with the experimental measurement of Hishida *et al.* (1986). These databases were used to evaluate the recent two-equation model of Nagano & Kim (1988), which is composed of k, ϵ, k_θ and ϵ_θ, and avoids previously used phenomenological assumptions for the turbulent Prandtl number by expressing eddy diffusivity using the timescale ratio of the dynamic and scalar fields. The difference in the exponent (p) of the timescale ratio determined in Nagano & Kim (1988) ($p = -\frac{1}{2}$) and in the statistical theory of Yoshizawa (1988) ($p = -2$) was investigated, and it was clearly demonstrated that both models have a low correlation with the LES database, and also that selecting $p \sim +1$ yields a much higher correlation. Dependence of the model performance on the method to input the scalar source was examined for all models using two types of scalar field boundary conditions in LES, together with fine and coarse grid resolutions. DNS was also conducted to confirm that the computed results were not distorted using LES turbulence models, yielding the same general conclusions for all experimental cases. To develop an eddy-diffusivity model which correctly satisfies the wall-limiting behaviour, a new model that smooths the bridging between the two extreme exponents of $p = -2$ and $p \sim 1$ is proposed, and was proven to be more numerically stable than when p is chosen equal to 1 throughout the channel. A critical comparison with the algebraic scalar flux model of Rogers *et al.* (1989) was

additionally conducted using these databases. A similarity of the correction functions in the eddy diffusivity in the proposed model and in RMR (1989) was apparent, with the feasible choice of the representative variable in this correction function being discussed. The importance of higher-order terms in anisotropic representation of scalar fluxes in the two-equation model was shown, and the relationship between anisotropic representation and AFM discussed. A possible use of third-order anisotropic representation terms as an alternative method for the reduction of eddy diffusivity near the wall instead of the conventional Van Driest damping function (Van Driest 1956) is suggested. Evaluation of the model coefficient for the pressure–scalar gradient term of Gibson & Launder (1976) was carried out, and higher correlation with the LES/DNS databases was obtained when the model constant for the 'rapid' part was chosen to be negative (~ -1.0), contrary to previous results of Launder (1975).

I am grateful to Dr M. M. Rogers for his valuable discussions and kindness in providing the unpublished data included in figure 17, and also for the valuable comments from Drs N. Kasagi and J. C. R. Hunt.

All computations were performed using the University of Tokyo Computer Center's HITAC S-820 model 80 System, with computational facilities being provided under a University of Tokyo/Hitachi Ltd Joint Research Program. This work was partially supported by Grant-in-Aid for Scientific Research nos. 01613002 and 02302043 from the Ministry of Education of Japan.

REFERENCES

Antonopoulos-Domis, M. 1981 Large-eddy simulation of a passive scalar in isotropic turbulence. *J. Fluid Mech.* **104**, 55–79.

Bardina, J., Ferziger, J. H. & Reynolds, W. C. 1980 Improved subgrid scale models for large eddy simulation. *AIAA paper* 80-1357.

Beguier, C., Dekeyser, I. & Launder, B. E. 1978 Ratio of scalar and velocity dissipation time scales in shear flow turbulence. *Phys. Fluids* **21**, 307–310.

Blackwelder, R. F. & Eckelmann, H. 1979 Streamwise vortices associated with the bursting phenomenon. *J. Fluid Mech.* **94**, 577–594.

Bremhorst, K. & Bullock, K. J. 1970 Spectral measurements of temperature and longitudinal velocity fluctuations in fully developed pipe flow. *Intl J. Heat Mass Transfer* **13**, 1313–1329.

Champagne, F. H., Harris, V. G. & Corrsin, S. 1970 Experiments on nearly homogeneous turbulent shear flow. *J. Fluid Mech.* **41**, 81–139.

Clark, J. A. 1968 A study of incompressible turbulent boundary layers in channel flow. *Trans. ASME* D: *J. Basic Engng* **90**, 455–468.

Clark, R. A., Ferziger, J. H. & Reynolds, W. C. 1977 Evaluation of subgrid-scale models using an accurately simulated turbulent flow. *J. Fluid Mech.* **91**, 1–16.

Elgobashi, S. E. & Launder, B. E. 1983 Turbulent time scales and the dissipation rate of temperature variance in the thermal mixing layer. *Phys. Fluids* **26**, 2415–2419.

Gibson, M. M. & Launder, B. E. 1976 On the calculation of horizontal, turbulent, free shear flows under gravitational influence. *Trans. ASME* C: *J. Heat Transfer* **98**, 81–87.

Gibson, M. M., Verriopoulos, C. A. & Nagano, Y. 1982 Measurements in the heated turbulent boundary layer on a mildly curved convex surface. In *Turbulent Shear Flows 3* (ed. L. J. S. Bradbury, F. Durst, B. E. Launder, F. W. Schmidt & J. H. Whitelaw), pp. 80–95. Springer.

Grötzbach, G. & Schumann, U. 1979 Direct numerical simulation of turbulent velocity, pressure and temperature fields in channel flows. In *Turbulent Shear Flows 1* (ed. F. Durst, B. E. Launder, F. W. Schmidt & J. H. Whitelaw), pp. 370–385. Springer.

Hinze, J. O. 1959 *Turbulence*. McGraw-Hill.

HISHIDA, M., NAGANO, Y. & TAGAWA, M. 1986 Transport processes of heat and momentum in the wall region of turbulent pipe flow. *Proc. 8th Intl Symp. on Heat Transfer Conf. San Francisco, California*, vol. 3, pp. 925–930.

HORIUTI, K. 1985 Large eddy simulations of turbulent channel flow by one-equation modeling. *J. Phys. Soc. Japan* **54**, 2855–2865.

HORIUTI, K. 1987 Comparison of conservative and rotational forms in large eddy simulation of turbulent channel flow. *J. Comp. Phys.* **71**, 343–370.

HORIUTI, K. 1988 Numerical simulation of turbulent channel flow at low and high Reynolds numbers. In *Transport Phenomena in Turbulent Flows: Theory, Experiment and Numerical Simulation* (ed. M. Hirata & N. Kasagi), pp. 743–755. Hemisphere.

HORIUTI, K. 1989 The role of the Bardina model in large eddy simulation of turbulent channel flow. *Phys. Fluids* A **1**, 426–428.

HORIUTI, K. 1990 Higher order terms in anisotropic representation of the Reynolds stresses. *Phys. Fluids* A **2**, 1708–1710.

HORIUTI, K. 1991*a* A proper energy scale in the subgrid scale eddy viscosity of large eddy simulation. Submitted to *Phys. Fluids* A.

HORIUTI, K. 1991*b* Validation of subgrid scale models for large eddy simulation of passive scalar. In preparation.

HUSSAIN, A. K. M. F. & REYNOLDS, W. C. 1975 Measurements in fully developed turbulent channel flow. *Trans. ASME* I: *J. Fluids Engng* **97**, 568–578.

KIM, J., MOIN, P. & MOSER, R. 1987 Turbulent statistics in fully developed channel flow at low Reynolds number. *J. Fluid Mech.* **177**, 133–166.

KIM, J. 1988 Investigation of heat and momentum transport in turbulent flows via numerical simulations. In *Transport Phenomena in Turbulent Flows: Theory, Experiment and Numerical Simulation* (ed. M. Hirata & N. Kasagi), pp. 715–729. Hemisphere.

KLINE, S. J., REYNOLDS, W. C., SCHRAUB, F. A. & RUNSTADLER, P. W. 1967 The structure of turbulent boundary layers. *J. Fluid Mech.* **30**, 741–773.

KLEBANOFF, P. S. 1954 Characteristics of turbulence in a boundary layer with zero pressure gradient. *NACA Tech. Note* 3178.

LAUFER, J. 1951 Investigation of turbulent flow in a two-dimensional channel. *NACA Rep.* 1053.

LAUNDER, B. E. 1975 On the effects of a gravitational field on the turbulent transport of heat and momentum. *J. Fluid Mech.* **67**, 569–581.

LESLIE, D. C. 1973 *Developments in the Theory of Turbulence*. Oxford University Press.

MANSOUR, N. N., KIM, J. & MOIN, P. 1988 Reynolds-stress and dissipation-rate budgets in a turbulent channel flow. *J. Fluid Mech.* **194**, 15–44.

MOIN, P. & KIM, J. 1982 Numerical investigation of turbulent channel flow. *J. Fluid Mech.* **118**, 341–377.

MYONG, H. K. 1988 Fundamental studies on a two-equation turbulence model for numerical predictions of wall-bounded shear flow and heat transfer. PhD dissertation, Dept of Mechanical Engineering, University of Tokyo.

NAGANO, Y. & HISIDA, M. 1985 Production and dissipation of turbulent velocity and temperature fluctuations in fully developed pipe flow. *Proc. 5th Symp. on Turb. Shear Flows, Cornell University, Ithaca*, pp. 1419–1424.

NAGANO, Y. & KIM, C. 1988 A two-equation model for heat transport in wall turbulent shear flows. *Trans. ASME* C: *J. Heat Transfer* **110**, 583–589.

NAGANO, Y., TAGAWA, M. & NIIMI, M. 1988 A two equation model for heat transfer taking into account the near-wall limiting behaviour of turbulence. *Proc. 25th Natl Heat Transfer Symp. of Japan*, vol. 2, pp. 166–168 (in Japanese).

NAKAJIMA, M., FUKUI, K., UEDA, H. & MIZUSHINA, T. 1980 Buoyancy effects of turbulent transport in combined free and forced convection between vertical parallel plates. *Intl J. Heat Mass Transfer* **23**, 1325–1336.

NEWMAN, G. R., LAUNDER, B. E. & LUMLEY, J. L. 1981 Modelling the behaviour of homogeneous scalar turbulence. *J. Fluid Mech.* **111**, 217–232.

NISIZIMA, S. & YOSHIZAWA, A. 1987 Turbulent channel and Couette flows using an anisotropic $k-\epsilon$ model. *AIAA J.* **25**, 414–420.

PIOMELLI, U., MOIN, P. & FERZIGER, J. H. 1988 Model consistency in large eddy simulation of turbulent channel flows. *Phys. Fluids* **31**, 1844–1891.

POPE, S. B. 1983 Consistent modeling of scalars in turbulent flows. *Phys. Fluids* **26**, 404–408.

ROGERS, M. M., MANSOUR, N. N. & REYNOLDS, W. C. 1989 An algebraic model for the turbulent flux of a passive scalar. *J. Fluid Mech.* **203**, 77–101.

RUBINSTEIN, R. & BARTON, J. M. 1990 Nonlinear Reynolds stress models and the renormalization group. *Phys. Fluids* A **2**, 1472–1476.

RUBINSTEIN, R. & BARTON, J. M. 1991 Renormalization group analysis of anisotropic diffusion in turbulent shear flows. *Phys. Fluids* A **3**, 415–421.

SCHUMANN, U. 1975 Subgrid scale model for finite difference simulation of turbulent flows in plane channels and annuli. *J. Comp. Phys.* **18**, 376–404.

SMAGORINSKY, J. 1963 General circulation experiments with the primitive equations. I. The basic experiment. *Mon. Weather Rev.* **91**, 99–164.

SPEZIALE, C. G. 1987 On nonlinear K-l and K-ϵ models of turbulence. *J. Fluid Mech.* **178**, 459–475.

TAVOULARIS, S. & CORRSIN, S. 1981 Experiments in nearly homogeneous turbulent shear flow with a uniform mean temperature gradient. *J. Fluid Mech.* **104**, 311–367.

TSAI, H. M., VOKE, P. R. & LESLIE, D. C. 1987 Numerical investigation of a combined free and forced convection turbulent channel flow. *Proc. 6th Symp. of Turb. Shear Flows, Toulouse*, pp. 531–536.

VAN DRIEST, E. R. 1956 On turbulent flow near a wall. *J. Aero. Sci.* **23**, 1007–1011.

WASSEL, A. T. & CATTON, I. 1973 Calculation of turbulent boundary layers over flat plates with different phenomenological theories of turbulence and various turbulent Prandtl number. *Intl J. Heat Mass Transfer* **16**, 1547–1563.

WEBSTER, C. A. G. 1964 An experimental study of turbulence in a density stratified shear flow. *J. Fluid Mech.* **19**, 221–245.

YOSHIZAWA, A. 1978 A governing equation for the small-scale turbulence. II. Modified DIA approach and Kolmogorov's $-\frac{5}{3}$ power law. *J. Phys. Soc. Japan* **45**, 1734–1740.

YOSHIZAWA, A. 1979 Statistical approach to inhomogeneous turbulent diffusion: general formulation and diffusion of a passive scalar in wall turbulence. *J. Phys. Soc. Japan* **47**, 659–662.

YOSHIZAWA, A. 1985 Statistical analysis of the anisotropy of scalar diffusion in turbulent shear flows. *Phys. Fluids* **28**, 3226–3231.

YOSHIZAWA, A. 1988 Statistical modelling of passive-scalar diffusion in turbulent shear flow. *J. Fluid Mech.* **195**, 541–555.